GEOLOGICA CARPATHICA, JUNE 2021, 72, 3, 253–281 https://doi.org/10.31577/GeolCarp.72.3.5

Review article

Perlite deposits of the Central Slovakia Volcanic Field (Western Carpathians): Geology and properties

JAROSLAV LEXA[1,✉], PETER VARGA[2], PETER UHLÍK[2], PETER KODĚRA[2], ADRIÁN BIROŇ[3] and MICHAL RAJNOHA[2]

[1]Earth Science Institute, Slovak Academy of Sciences, Dúbravská cesta 9, 840 05 Bratislava, Slovakia; ✉geoljalx@savba.sk
[2]Department of Mineralogy, Petrology and Economic Geology, Faculty of Natural Sciences, Comenius University in Bratislava, Mlynská dolina, Ilkovičova 6, 842 15 Bratislava, Slovakia; peter.vargamineraly@gmail.com, peter.uhlik@uniba.sk, peter.kodera@uniba.sk, michal.dionyzos@gmail.com
[3]Earth Science Institute, Slovak Academy of Sciences, Ďumbierska 1, 974 11, Banská Bystrica, Slovakia; biron@savbb.sk

(Manuscript received January 24, 2021; accepted in revised form May 4, 2021; Associate Editor: Igor Broska)

Abstract: Perlites in the Central Slovakia Volcanic Field are associated with with rhyolite dykes, cryptodomes, extrusive domes, coulées and volcanoclastic rocks of the Jastrabá Fm. (12.3–11.4 Ma). From numerous occurrences only the Lehôtka pod Brehmi (LPB) and Jastrabá (JST) represent deposits of economic interest. The LPB deposit exploits a pile of extruded hyaloclastite breccia composed of grey porous and dark dense fragments. The JST deposit exploits glassy rhyolite breccia composed of grey porous fragments associated with an extrusive dome/coulée. The perlites at both deposits are peraluminous, calc-alkaline of the high-K type, poor in phenocrysts (around 5 %) of plagioclase, biotite and minor amphibole (LPB) or sanidine/anorthoclase (JST). Glass at both deposits is silica rich (75.4–79.5 wt. % dry) with Al_2O_3, K_2O and Na_2O as other major constituents. It is inhomogeneous showing domains enriched in Na_2O or K_2O. Glass water content (3.0–6.0 wt. %) shows a weak positive correlation with its silica content and a negative correlation with its Na_2O content. Perlites show porosities of 5–16 % (dark dense), 16–30 % (grey porous) and 30–44 % (pale grey pumiceous). Narrow stretched pores represent remnants after outgassing of ascending magma while open undeformed pores grew at a low pressure before quenching. The transformation of volcanic glass into perlite took place owing to the hydration by heated fluids of meteoric origin. The hydration was supported by a significant porosity with interconnected pores and by sustained elevated temperature. Perlites at both deposits show a low content of tightly-bound water and a low Na/K ratio. These properties are responsible for their relatively low degree of expansion. On the other hand, due to the same reason, the perlites have a good mechanical stability.

Keywords: rhyolite monogenetic volcanoes, perlite, petrography, mineralogy, geochemistry, genesis, properties.

Introduction

Perlite is hydrated silicic volcanic glass with a water content of 3 to 5 wt. % (Barker & Santini 2006). The colour of raw perlite is pale grey to glossy black reflecting pumiceous, granular and/or onion skin textures (Barker & Santini 2006). The origin of perlites is related to extrusive volcanic activity in the terrestrial environment (Bouška et al. 1993; Yanev 2008). Perlites are associated variably with lava flows, extrusive domes, dykes, sills (Richey 1961; Lange & Heide 1996; Nasedkin 1996; Yanev 2008), cryptodomes, laccoliths, intrusive sheets (Yanev 2003, 2008), subglacial bodies (Denton et al. 2012) and hyaloclastite breccias (Yanev 2003; Denton et al. 2012). Perlites chemically consist generally of 69–75 % SiO_2, 12–14 % Al_2O_3, 3–4.6 % Na_2O, 3.8–5 % K_2O, 0.5–1.6 % CaO, 0.6–1.8 % Fe_2O_3 with small amounts of TiO_2 and MgO (Breese & Barker 1994). Phenocrysts of plagioclase, K-feldspar, biotite and rare quartz or amphibole are typically present in vitreous matrix (e.g. Yanev 2008; Zelenka 2013).

Perlite is an important raw material having unique properties especially after processing. Major industrial utilization of perlite is in the form of expanded perlite, which is produced by a quick heating of ground natural perlite at 800–1200 °C (Šalát & Ončáková 1964; Breese & Barker 1994; Barker & Santini 2006). Expanded perlite can be characterized as a pale to white granular and foamy material with extremely low density (30–240 kg/m^3), high porosity and high specific surface area. Its physical–chemical properties induce high sound and thermal insulation capacity, heat resistance, chemical inertness and high filtration ability of expanded perlite. These properties lead to its application in various branches of the economy, mainly in the building industry but also in the food industry, agriculture and environmental protection (Breese & Barker 1994; Barker & Santini 2006). Important European perlite deposits are located in Greece, Turkey, Bulgaria, Italy, Iceland, Hungary and Slovakia (Singh 2020). In the Slovak Republic perlite is registered at five deposits with a stock of about 30 million tonnes (Kúšik et al. 2019).

Perlite deposits of the Central Slovakia Volcanic Field (CSVF, Fig. 1) were explored from the early 1960s to the end of the twentieth century (Beňo & Očenáš 1962; Šalát & Ončáková 1964; Zuberec & Sýkora 1976; Kraus et al. 1980;

Zuberec et al. 1980; Hroncová 1989, 1994; Hroncová et al. 1991). Detailed exploration at the Lehôtka pod Brehmi (LPB) deposit (Beňo & Očenáš 1962) has enabled exploitation of the deposit in an open quarry since the year 1963. Annual production of perlite range from 17 to 48 kt during the last five years (Kúšik et al. 2019). The Jastrabá (JST) deposit was discovered during a prospecting campaign in the years 1974–1980 (Zuberec et al. 1980; Kraus et al. 1980) aimed at checking potential reserves of perlite at other localities of the CSVF. With proven and probable reserves estimated at 30 Mt it represents the biggest deposit of perlite in the Western Carpathians (Zuberec et al. 1980; Hroncová 1989, 1994; Hroncová et al. 1991). At the present time, the deposit is ready for the beginning of exploitation. Recent exploration and exploitation at both perlite deposits are operated by the company LBK PERLIT s. r. o. (http://www.lbkperlit.sk/).

Due to its quantity and quality, perlite is still one of the promising raw materials of Slovakia. The aim of this paper is to summarize new results concerning perlites at the LPB and JST deposits after a research gap of two decades. Perlites will be characterized primarily from the point of view of mineralogy–petrology, chemical composition, water content, its type, porosity and the geological position of the deposits. The qualitative perlite characterization is an important input for processing as well as for creation of a genetic model.

Methods of investigation

Field work included a detailed geological mapping of both perlite deposits, careful documentation of lithology and collection of representative samples for laboratory investigation. Microscopic study of polished sections in transmitted light was the next step. Porosity was also studied using microprobe BSE images, by scanning electron microscopy (SEM) using N_2 adsorption and by X-ray computed microtomography (Varga et al. 2019). The chemical composition of perlite was established by ICP-ES and ICP-MS methods. Electron-microprobe analyses (EMPA) of minerals and glass were carried out on the CAMECA SX100 probe. Mineralogical composition was established by X-ray diffractometry. Loss on ignition (LOI) was measured in a muffle furnace at 950 °C. The loss of perlite water during thermal treatment was studied by thermogravimetric (TG), differential thermal analyses (DTA) and by LOI at different temperatures and time intervals (Varga et al. 2019). Details of methodology are treated in the El. Suppl. 1.

Geological setting of the deposits

Deposits and occurrences of perlites in the Central Slovakia Volcanic Field (CSVF) are related to products of rhyolite volcanic activity of the Jastrabá Fm. (Konečný et al. 1983, 1998; Lexa et al. 1998). Rhyolites of the Jastrabá Fm. represent, along with almost coeval high-alumina basalts, the youngest volcanic products of the mostly andesitic volcanic field (Konečný et al. 1995) associated with the back-arc extension of the Carpathian arc (Lexa & Konečný 1998). Results of radiometric dating of rhyolites by K–Ar, as well as Rb–Sr methods fall in the interval 12.3±0.4–11.4±0.4 Ma (Lexa & Pécskay 2010; Chernyshev et al. 2013). Rhyolites of the Jastrabá Fm. extend over an area 50×20 km and associate with a system of N–S to NE–SW trending faults, including marginal faults of the intravolcanic Žiar basin (surroundings of the town of Žiar nad Hronom in the Fig. 1). Their activity was contemporaneous with subsidence of the basin and uplift of resurgent horsts in the Štiavnica stratovolcano caldera south of the basin and in the Kremnica graben north of the basin (Fig. 1). In uplifted areas of the horsts only dikes and extrusive dome roots appear in association with epithermal hydrothermal systems, while in less eroded parts of the formation outside of the Žiar basin dykes, extrusive domes and dome-flows associate with sporadic remnants of tuffs and epiclastic breccias (Konečný et al. 1998; Lexa et al. 1998; Lexa in Demko et al. 2010; Lexa & Pošteková 2012). Within the Žiar basin the formation shows thicknesses of up to 300 m. A rhyolite dome/flow complex with associated pyroclastic and epiclastic volcanic rocks is exposed in the S, SE, E and NE parts of the basin (Fig. 1). The complex rests on volcanic/sedimentary fill of the basin showing thicknesses of 2000–2500 m (Lexa et al. 1998). The uppermost 600–800 m of the fill is represented by lacustrine and fluvial sedimentary rocks including gravel and sand horizons (Konečný et al. 2003) – aquifers that stimulated initial phreatomagmatic explosive activity of rising rhyolite magma (Lexa & Pošteková 2012). The complex with multiple vents localized especially at a system of marginal faults of the Žiar basin is built up by a succession of dykes, cryptodomes, extrusive domes, dome-flows and lava flows with associated phreatomagmatic agglomerates and tuffs, hyaloclastite and extrusive breccias, proximal facies aprons of block and ash flow deposits and epiclastic breccias, and distal facies accumulations of epiclastic volcanic breccias, sandstones and reworked tuffs including horizons of fluvial conglomerates (Lexa et al. 1998; Lexa in Demko et al. 2010; Lexa & Pošteková 2012). Perlite occurs: (1) at contacts of dykes, cryptodomes and extrusive dome roots with surrounding rocks in thickness of few metres, passing inward into rhyolites with spherulitic, felsospherulitic and felsitic groundmass; (2) in the form of perlitic extrusive breccias at the top and/or margins of extrusive domes and dome-flows; (3) in the form of perlitic hyaloclastite breccias; (4) as fragments in block and ash flow breccias and epiclastic volcanic breccias; (5) as fragments in pyroclastic rocks. Among the numerous occurrences of perlite in the CSVF only two are large enough to represent exploitable perlite deposits – Lehôtka pod Brehmi and Jastrabá.

Geology of the deposits

Both studied perlite deposits represent parts of monogenetic rhyolite volcanoes (cf. Lexa et al. 2010) situated on the SE to E marginal fault system of the Žiar basin (Fig. 1). While

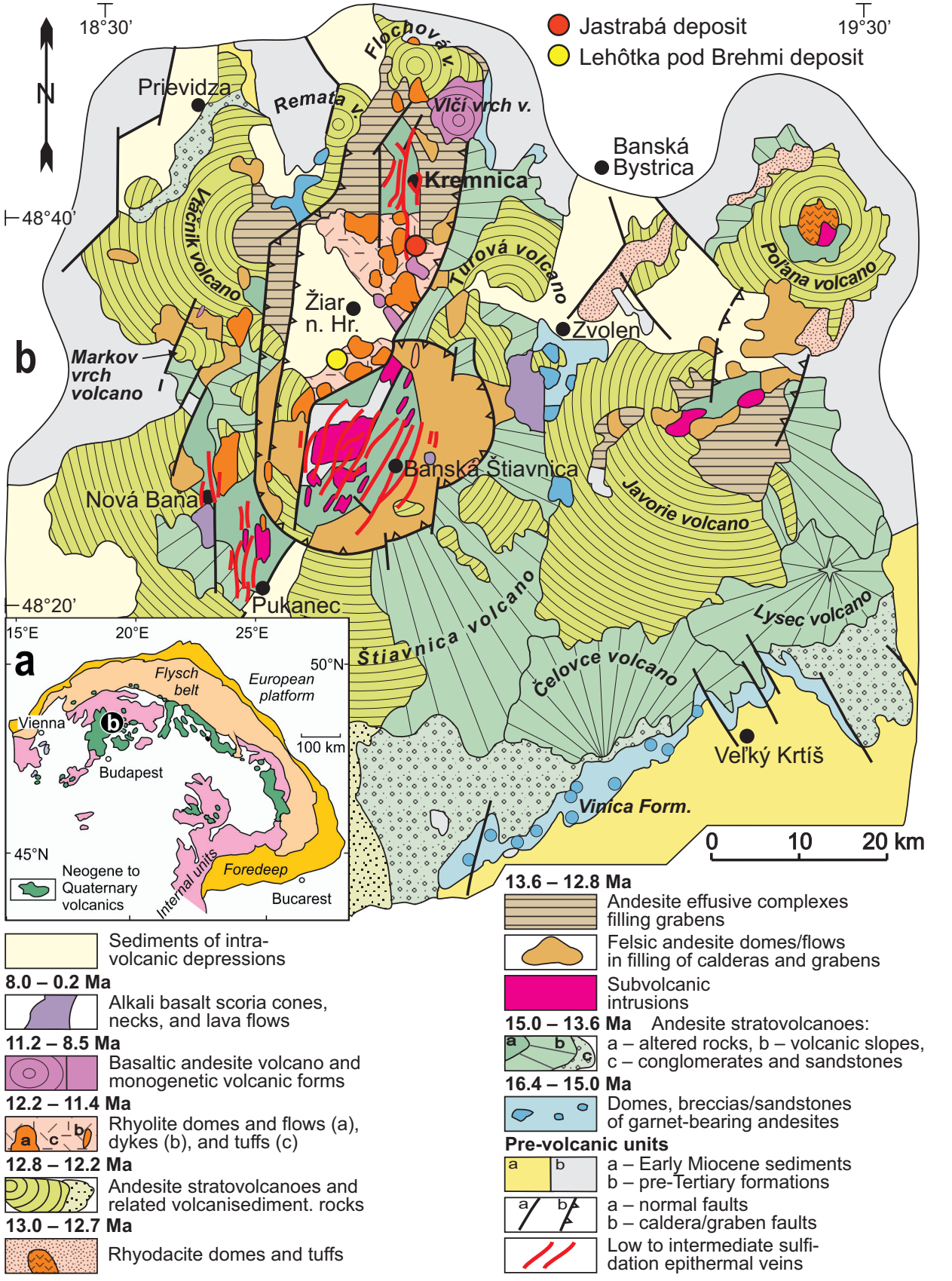

Fig. 1. a — Position of the Central Slovakia Volcanic Field (CSVF) among Neogene to Quaternary volcanic formations of the Carpathian arc. **b** — Structural scheme of the Central Slovakia Volcanic Field including localization of the studied perlite deposits among rocks of the Jastrabá Formation (12.2–11.4 Ma), modified after Konečný et al. (1995) and Chernyshev et al. (2013).

the JST deposit represents a common deposit type of extrusive dome-flow related perlitic breccia, the LPB deposit represents an unusual deposit type of perlitized extruded hyaloclastite breccia. Naturally, they differ in their geology, evolution and perlite properties. Field photographic documentation and details of lithology are in the El. Suppl. 2.

The Lehôtka pod Brehmi deposit

The rhyolite monogenetic volcano that hosts the LPB perlite deposit shows a complex structure and evolution (Fig. 2). Phreatomagmatic tuffs and fine pyroclastic breccias rich in andesite fragments/pebbles represent the oldest, unexposed unit (known from boreholes) that rests on older andesites (Beňo & Očenáš 1962) and sediments of the Žiar basin (Forgáč et al. 1974). In the eastern part of the deposit, a dome formed by extruded hyaloclastite breccia represents the overlying unit. Locally, the breccia includes irregular, partially brecciated thin tongues of coherent glassy lava. This body of extrusive perlitic breccia has been an object of exploitation since the year 2017.

The succession of monogenetic volcano units continues in its western part and surroundings with a thick unit of phreatomagmatic tuffs and fine pyroclastic breccias including a lesser or rare admixtures of andesite and nonvolcanic rock pebbles (Fig. 2). Fine breccias and lapilli tuffs with rare blocks dominate in the proximal facies that forms remnants of a pyroclastic ring. Outward dipping strata in the north pass southward into inward dipping strata of the assumed maar (as indicated in the section of the Fig. 2). Corresponding distal facies tuffs east of the volcano are mostly fine, stratified and well sorted. Massive beds of fine pyroclastic breccia are rare.

Phreatomagmatic fine breccias and lapilli tuffs of the pyroclastic ring are covered and laterally succeeded to the south by a thick accumulation of coarse perlitic extrusive breccia of the hyaloclastite type (Lexa 1971) – an object of past exploitation (Fig. 2). It is exposed also south-westward of the deposit in surroundings of the Szabóova skala. As in the underlying pyroclastic rocks, perlite fragments and blocks are dominantly porous to pumiceous of pale grey colour, with less frequent dark to black fragments of dense perlite. The proportion of dark dense fragments increases bellow overlying lava flows. In the western part of the deposit, the extrusive perlitic breccia is covered conformably by two lava flows, dipping 35° north and 30° northwest, respectively (Fig. 2). Rhyolite of the lava flows is glassy and perlitic, dark and dense, similar to dark fragments in the underlying extrusive breccia. The succession in the western part of the deposits continues with a second horizon of extrusive perlitic breccia, in this case relatively enriched with fragments of dark dense perlite. The topmost few metres of the breccia show a decrease in the size of fragments and increasing proportion of fine matrix. Laterally, this horizon passes into accumulation of reworked material east and west of the deposits – fine to coarse epiclastic volcanic breccias (Fig. 2). Tuffs composed dominantly of perlitic material represent the uppermost unit of the monogenetic volcano. They are well sorted and stratified, showing mantle bedding conformable with morphology of underlying extrusive breccia accumulation. They also extend east of the volcano (Fig. 2). The described succession of the monogenetic volcano units was subsequently levelled by erosion and covered by slightly younger sub-horizontal accumulation of fluvial conglomerates and sandstones (Fig. 2). At the south-western and southern parts of the volcano (beyond limits of the deposit) there are two rhyolite cryptodomes that are emplaced in extrusive perlitic breccias and underlying phreatomagmatic pyroclastic rocks (Fig. 2).

The Jastrabá deposit

A simple monogenetic rhyolite volcano hosting the JST perlite deposit evolved on top of older members of the rhyolitic Jastrabá Fm. These are different westward and eastward of a fault that served as a conduit for ascending rhyolite lava (Fig. 3). The exact position of the fault follows from the asymmetric structure of the Jastrabá skala extrusive dome (see below) and orientation of basaltic dykes emplaced along this fault south of the volcano. West of the fault there is a thick succession of zeolitized distal facies phreatomagmatic tuffs with reddish to pale felsitic rhyolite cryptodome that is affected by land-sliding. Glassy hyaloclastite breccias at margins of the cryptodome are also zeolitized. East of the fault there is a thick succession of unaltered distal facies phreatomagmatic tuffs that rests upon sediments of the Žiar basin at the depth of around 200 m (Lexa et al. 1998). The monogenetic volcano itself is represented by an extrusive dome-flow, related extrusive breccias and a fan of block and ash flow deposits, tuffs and epiclastic volcanic breccias that nowadays occur in an inverted mutual position (Fig. 3 section) thanks to a gradual growth of the dome-flow.

The asymmetric dome with its centre at the Jastrabá skala turns into short coulées (dome-flows) oriented in direction 25° (a thinner and longer one – around 500 m) and 115° (a thicker and shorter one – around 300 m). Orientation of flow banding follows a contact with older rocks at the base of cliffs on the western side of the dome and dips roughly towards the centre of the dome elsewhere (Fig. 3). It is rather flat (5°–15°) at the end of the northern coulée. At the eastern side of the volcano the coulées rest on a thick unit of coarse to blocky perlitic extrusive breccias that represent perlite resources of the deposit (Fig. 3). These breccias rest on and grade laterally into a fan of block and ash flow deposits, fall and/or surge type tuffs and fine to coarse epiclastic volcanic breccias.

Macroscopic characterization of perlite samples

All of the studied samples are portrayed in the El. Suppl. 3, including their macro- and microphotographs and BSE images. Two essential textural varieties of perlite occur in the western part of the LPB deposit. Porous to pumiceous perlite is of pale grey colour, with macroscopically visible pores (Fig. 4A).

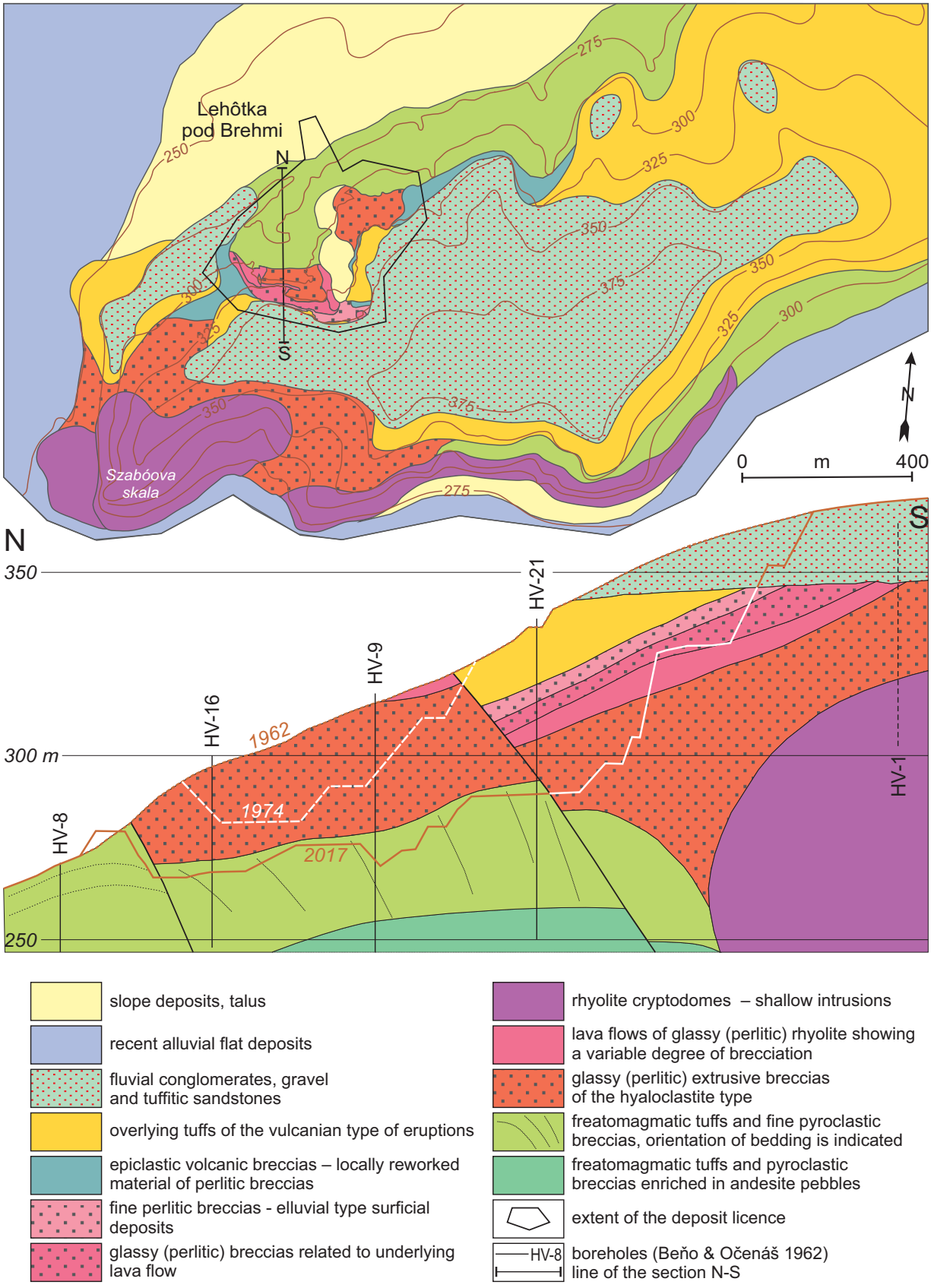

Fig. 2. Geological map of the Lehôtka pod Brehmi perlite deposit and surroundings (state in the year 2017) and geological section in the western part of the deposit (compiled by J. Lexa using borehole logs of Beňo & Očenáš 1962). In the section surface configurations in different years of geological mapping and exploitation are indicated.

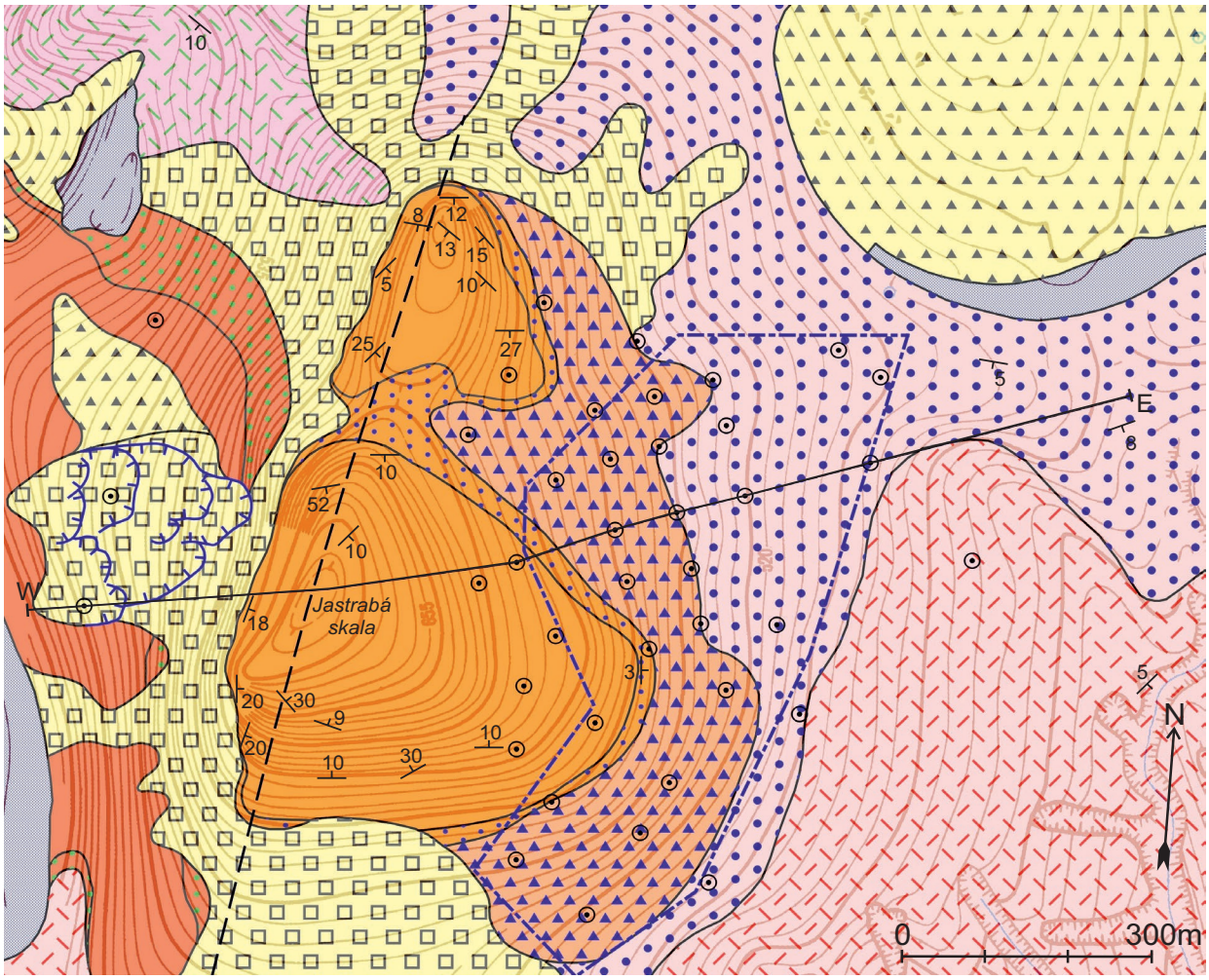

Fig. 3. Geological map of the Jastrabá perlite deposit and surroundings and geological section across the central part of the deposit (compiled by J. Lexa using borehole logs and geological map of Zuberec et al. 1980).

Some of them show a flow-oriented texture and/or flow banding. Dense perlite is of the dark grey to black colour (Fig. 4B), variably with vitreous lustre, conchoidal fracture and polygonal disintegration with curviplanar edges. Only a few of the dark dense perlites also show the typical onion skin perlitic texture. Less frequent transitional varieties of moderately porous perlite of grey colour have been observed too (Fig. 4D). In the exploited perlitic breccia the pale and dark perlite fragments are embedded in matrix of unsorted medium-grain perlite detritus (Fig. 4C) that represents 20 to 50 % of breccia and its proportion is variable throughout the deposit. The size of grains is variable. However, granularity is relatively homogenous in the whole deposit (Fig. 5). Extrusive perlitic breccia in the eastern part of the deposit is formed of almost uniform grey porous perlite showing flow-banding (alternating darker and lighter bands). The proportion of the unsorted detritic matrix is in this case smaller.

Perlite fragments and blocks of the extrusive breccia that represents the resource of the JST deposit are quite uniform, pale grey to grey, porous to pumiceous (Fig. 6A and C), often showing the flow-oriented texture and/or flow banding (Fig. 6B). Unsorted matrix in the proportion 25–50 % (Fig. 6D) is composed of fine to coarse perlite detritus (Fig. 7).

Petrography, mineralogy and chemical composition of perlites

The perlites in the Jastrabá Fm. of the CSVF are phenocryst-poor rhyolites with hydrated glassy groundmass. They are spatially associated with rhyolites that show variably spherulitic, felso-spherulitic and/or felsitic groundmass. All of the Jastrabá Formation rhyolites are porphyritic with a variable proportion of plagioclase, sanidine, quartz, biotite and/or amphibole phenocrysts – plagioclase, sanidine–plagioclase, quartz–sanidine–plagioclase, plagioclase–sanidine and plagioclase–quartz–sanidine rhyolites have been distinguished (e.g. Hojstričová 1982; Lexa et al. 1997; Demko et al. 2010). Their phenocryst content varies mostly in the range 3–8 %. Based on the phenocryst assemblage, perlite of the LPB deposit represents the hydrated glassy type of plagioclase rhyolite, while perlite of the JST deposit represents the hydrated glassy type of quartz–sanidine–plagioclase rhyolite. In addition to the petrographic description below, the El. Suppl. 3 brings additional microphotographs and BSE images of evaluated samples.

Optical microscopy and microprobe observations

The perlites at both deposits show porphyritic texture with phenocrysts of plagioclase, biotite and sporadic amphibole (LPB, Fig. 8A–D) or rare quartz and sanidine (JST, Fig. 9A–E). Distribution of phenocrysts is not uniform, their content varies around 5 % in the LPB deposit (1.0–6.3 % plagioclase and 0.3–1.6 % biotite) and around 6 % in the JST deposit (3.0–4.5 % plagioclase, 0.5–1.0 % quartz, 0.5–1.0 % sanidine and 0.3–1.0 % biotite). The size of phenocrysts is highly variable with maximum at 2.5 mm for plagioclase, 1.5–2 mm for biotite and amphibole, 1 mm for quartz and 0.2 mm for sanidine microphenocrysts. Zircon, apatite, magnetite, ilmenite and rare allanite occur as tiny accessory minerals.

Plagioclase phenocrysts occur as solitary grains and subordinate glomeroporphyric aggregates, sometimes along with biotite. Plagioclase phenocrysts are mostly euhedral, often showing a partial resorption and irregular fractures (LPB – Fig. 8B, D; JST – Fig. 9A, B). Normal and/or oscillatory zoning with a general decrease of An content towards their margins is characteristic. Some of the plagioclase phenocrysts in perlite of the LPB deposit show resorbed cores of a relatively lower An content surrounded by an An enriched zone (Fig. 8B) while in perlite of the JST deposit plagioclase phenocrysts show rare cores enriched in An component. The An-poorer as well as An-enriched cores frequently enclose melt inclusions, sometimes in association with tiny biotite grains. The composition of plagioclase phenocrysts varies in the range An_{31} to An_{54} (LPB deposit), or An_{23} to An_{39} (JST deposit). The El. Suppl. 4 provides corresponding statistical parameters of feldspar composition and a projection to the feldspar ternary diagram.

In perlite of the JST deposit sanidine and minor anorthoclase form euhedral, sometimes skeletal microphenocrysts, that occur as solitary grains or rare aggregates with quartz (Fig. 9D). Sanidine is quite rich in the Ab component (25–39 %) that increases up to 75 % in anorthoclase grains (Table S3 and Fig. S1 in the El. Suppl. 4). Both, sanidine and anorthoclase are enriched in Ba. Quartz occurs as solitary euhedral bipyramidal grains (Fig. 9B), partially resorbed grains and as aggregates with plagioclase, sanidine or biotite.

Biotite phenocrysts are mostly euhedral, sometimes showing a partial resorption (LPB – Fig. 8C, D; JST – Fig. 9B, E). They occur as solitary grains, intergrown with plagioclase and amphibole or enclosed in plagioclase phenocrysts. Biotite phenocrysts enclose accessory zircon, apatite and ilmenite and frequently also melt inclusions (Fig. 8C). With the exception of one analysis richer in Mg and poorer in Fe, biotite phenocrysts in perlite of the LPB deposit show a restricted range of compositional variability close to the boundary of annite and siderophyllite. In perlite of the JST deposit only a smaller part of biotite phenocrysts shows a similar composition and majority of biotite phenocrysts shows a relative enrichment in Fe and impoverishment in Mg and Ti (Table S4 and Fig. S2 in the El. Suppl. 4). In porous perlites of both deposits biotite phenocrysts are variably affected by kaolinization along their cleavage planes (Fig. 9E) up to a complete replacement (Fig. 9B).

Amphibole phenocrysts occur only in dark dense perlites at margins of LPB volcano cryptodomes. Like other phenocrysts, they are euhedral or partially resorbed (Fig. 8D). Solitary grains dominate, but aggregates with biotite and/or plagioclase have been observed too. Their composition is variable, in diagrams they separate into two groups – Mg-hornblendes with low Ti and Al contents and tschermakites/Mg-hastingsites with high Ti and Al contents (Table S5 and Fig. S3 in the El. Suppl. 4).

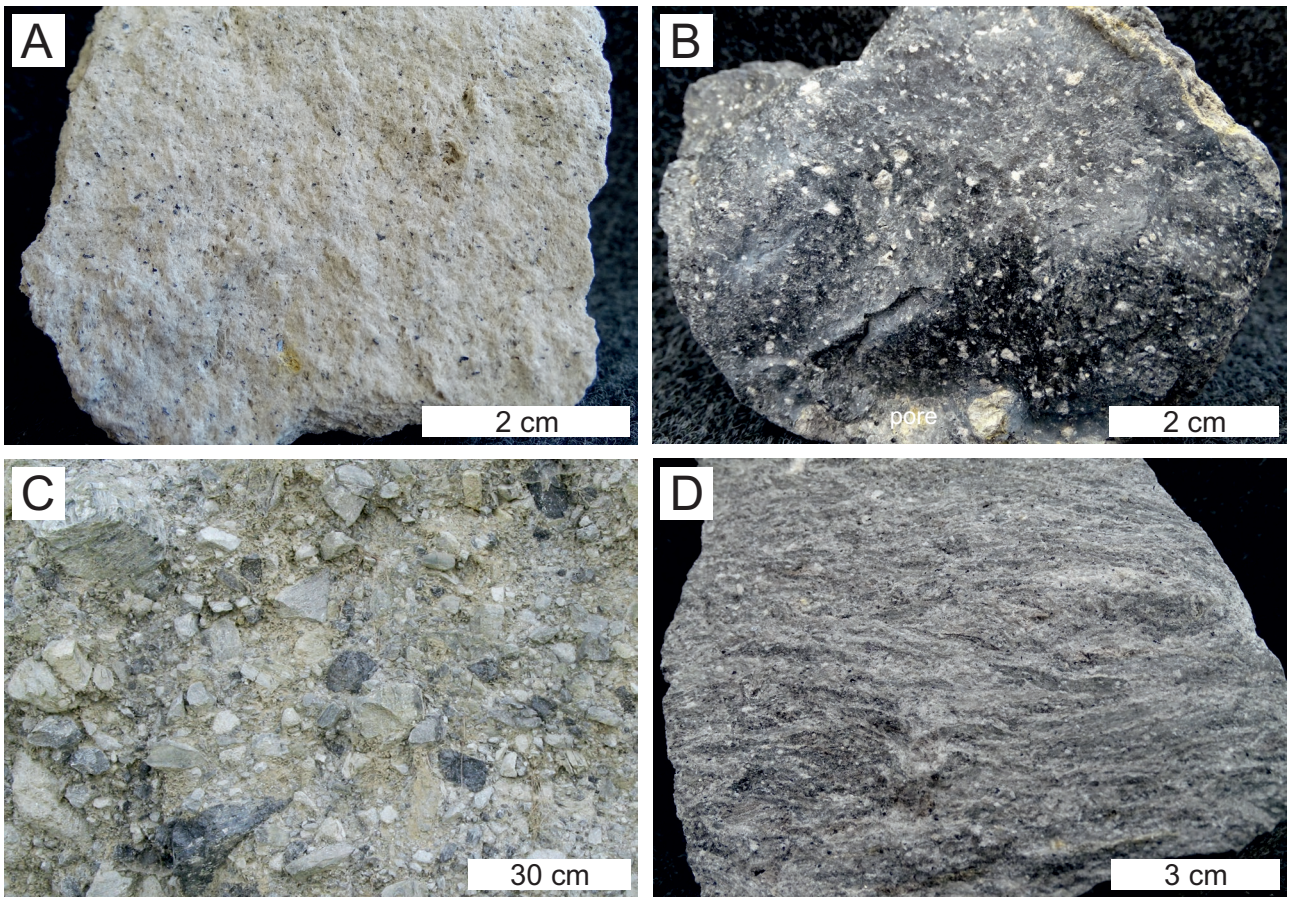

Fig. 4. Textural varieties of perlite from the Lehôtka pod Brehmi deposit: **A** — pale, porous to pumiceous perlite (sample PL-93a); **B** — dark, dense perlite showing conchoidal fractures (sample PL-248a); **C** — perlitic breccia with pale grey and dark fragments (locality PL-20); **D** — grey, porous perlite showing a flow-oriented texture (sample PL-254).

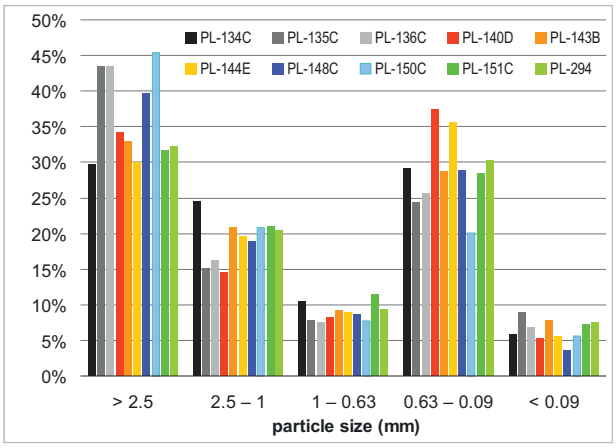

Fig. 5. Particle size distribution of granular matrix of perlitic extrusive breccia at the Lehôtka pod Brehmi perlite deposit.

Accessory minerals are dispersed in glassy groundmass or enclosed in phenocrysts. The most common accessory mineral is apatite. Stubby, prismatic or needle-like euhedral crystals reach up to 120 µm in diameter/length (Fig. 8C, H). Zircon is abundant and occurs as elongated, euhedral and subhedral crystals up to 50 µm in diameter. Euhedral to anhedral magnetite (up to 4.3 % TiO_2) grains up to 150 µm in diameter are common. Tiny ilmenite grains have been found especially as inclusions in biotite phenocrysts. In perlite of the JST deposit glass is affected locally by recrystallization to small spherulite-like aggregates of sanidine and quartz (Fig. 9F). Sporadic brown spherulites (sanidine and cristobalite with hematite pigment) have been observed in the southern part of the deposit.

While the phenocrysts assemblage and their composition in perlites of different lithological units of the LPB deposit are uniform, with the exception of cryptodomes also containing amphibole phenocrysts, their glassy groundmass shows a higher variability. Glass with no microlites or poor in microlites is characteristic of pale grey to grey porous and pumiceous perlites (Fig. 8B, E; El. Suppl. 3) and some dark dense perlites (Fig. 8C, D; El. Suppl. 3). Glass in the rest of dark dense perlites, especially of those from margins of cryptodomes, includes microlites of biotite, amphibole, pyroxene and accessory minerals in variable proportions, often in oriented bands of the fluidal texture (Fig. 8G, H). We have observed dark bands enriched in pyroxene microlites and trichytes in only a few samples. Glass in both types of perlites sometimes

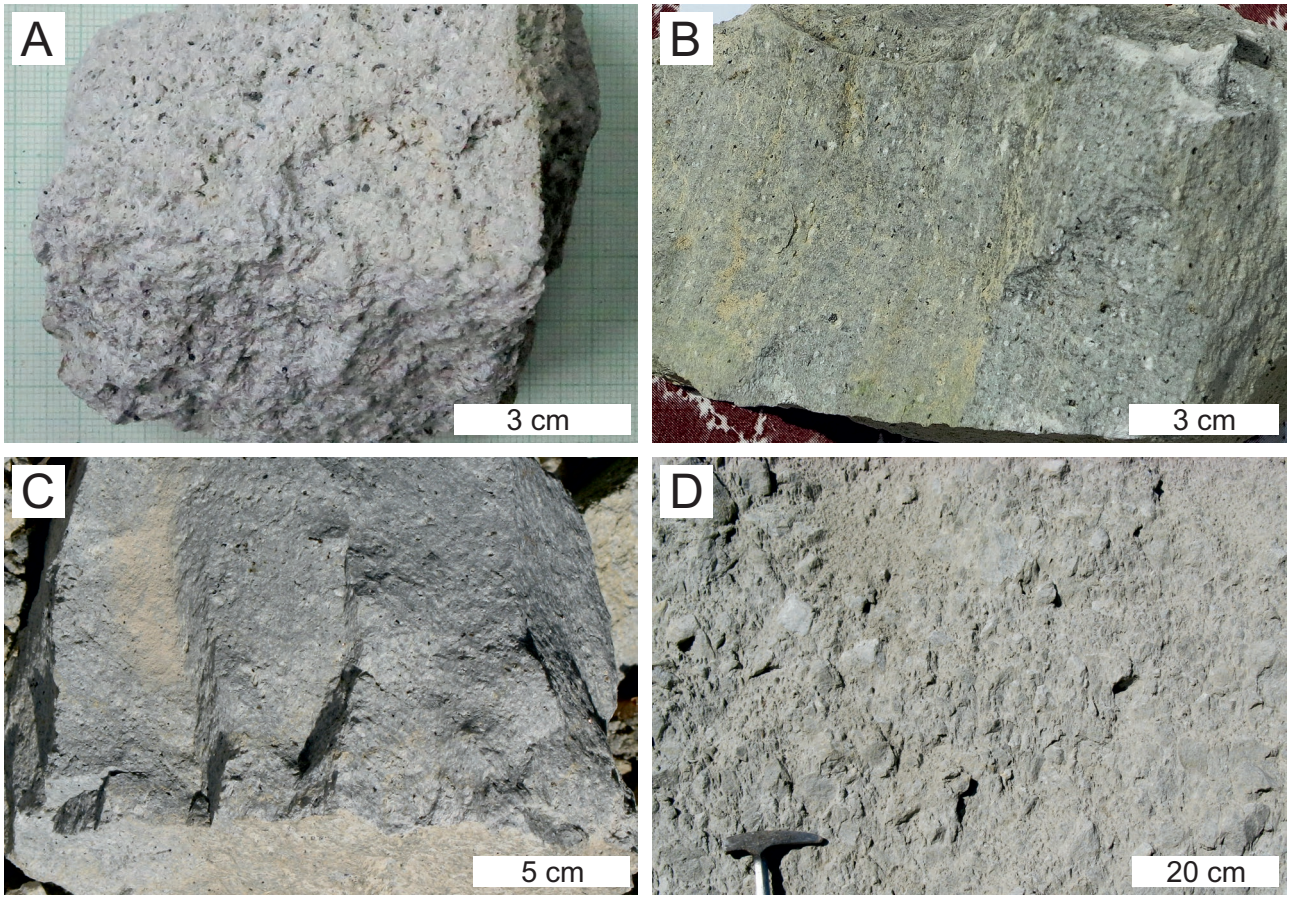

Fig. 6. Textural varieties of perlite from the Jastrabá deposit: **A** — pale, porous to pumiceous perlite (sample JS-26b); **B** — grey porous perlite showing a flow-oriented texture (locality JS-22); **C** — grey porous perlite, a piece from a chilled block with radial jointing (locality JS-4); **D** — perlitic extrusive breccia at the Jastrabá deposit (locality JS-26).

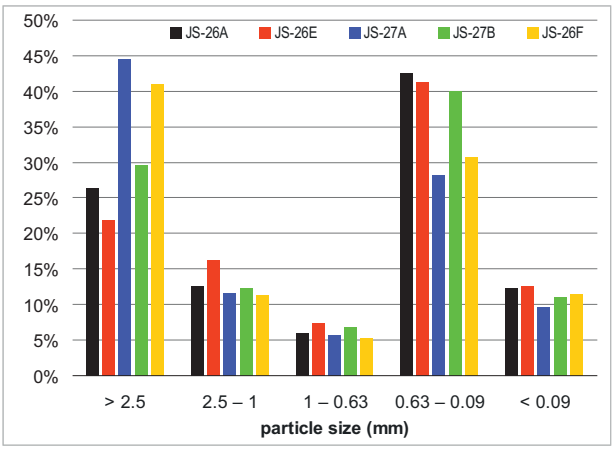

Fig. 7. Particle size distribution of granular matrix of perlitic extrusive breccia at the Jastrabá perlite deposit.

includes microlites (micro-phenocrysts) of feldspars up to 100 μm in diameter/length (Fig. 8F). Microlites of the plagioclase composition dominate, but microlites of the sanidine composition and rare microlites of the anorthoclase composition are present too. Groundmass glass of the JST deposit perlite is mostly free of or poor in microlites, represented by the above-mentioned accessory minerals. However, in some of the samples, glass is quite rich in microlites of alkali feldspars – anorthoclase and sanidine (Fig. 9F). Anorthoclase microlites show a high An content in the range 14.7–20.6 %. Sanidine microlites are mostly enriched in Ba. Feldspar microlite composition and its projection into the ternary feldspar diagram are given in Table S3 and Fig. S1 in the El. Suppl. 4. The composition of glass is treated in the text concerning chemical composition of perlites below.

Porosity of perlites

Porosity of perlites at the LPB and JST deposits has been studied by various methods including 3D X-ray tomography (Varga 2018; Varga et al. 2019). Here we summarize the most important aspects and illustrate the perlite porosity by BSE and SEM images (Fig. 10). Pores in glass cause a dispersion of light – pumiceous perlites are of pale grey colour, moderately porous ones are of grey colour and perlites with a limited or no porosity are of dark to black colour (El. Suppl. 3). Generally, two types of pores have been recognized: (1) Open, undeformed or slightly deformed large pores characteristic for

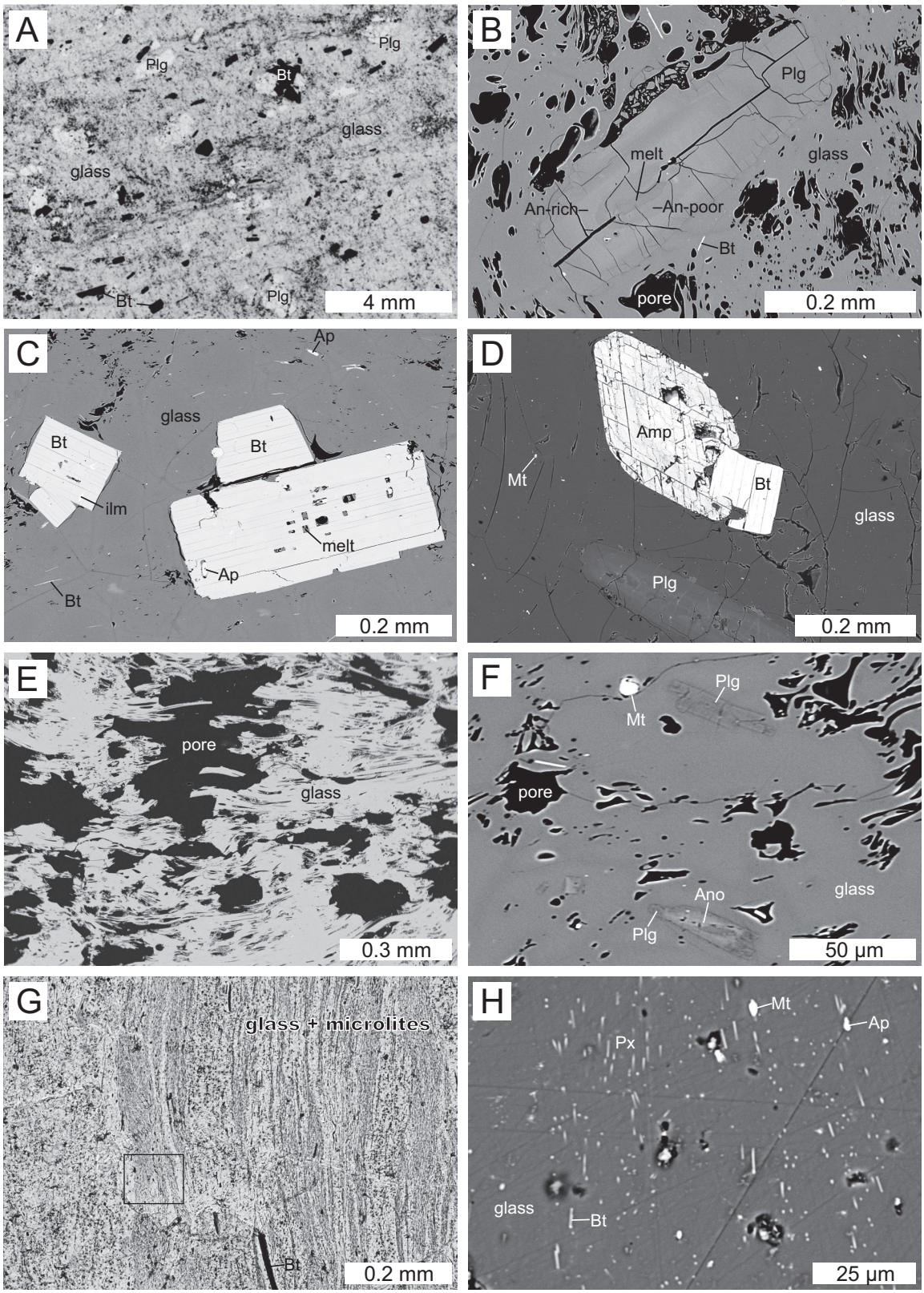

Fig. 8. Microphotographs (A, G) and BSE images of perlites from the Lehôtka pod Brehmi deposit: **A** — dark dense perlite (PL-20a); **B** — plagioclase phenocryst in porous glass showing resorbed An-poor core with a melt inclusion surrounded by an An-rich zone (PL-4a); **C** — biotite phenocrysts with inclusions of accessory apatite, ilmenite and melt (PL-19); **D** — phenocrysts of amphibole, biotite and plagioclase in dense glass (PH-16); **E** — porous glass groundmass with no microlites (PL-6b); **F** — microlites of anorthoclase, plagioclase and magnetite in porous glass groundmass (PL-19); **G** — groundmass of dark dense perlite rich in microlites (SS-5c); **H** — detail of the rectangle in G showing microlites of pyroxene, biotite, magnetite and apatite in a dense glass (SS-5c).

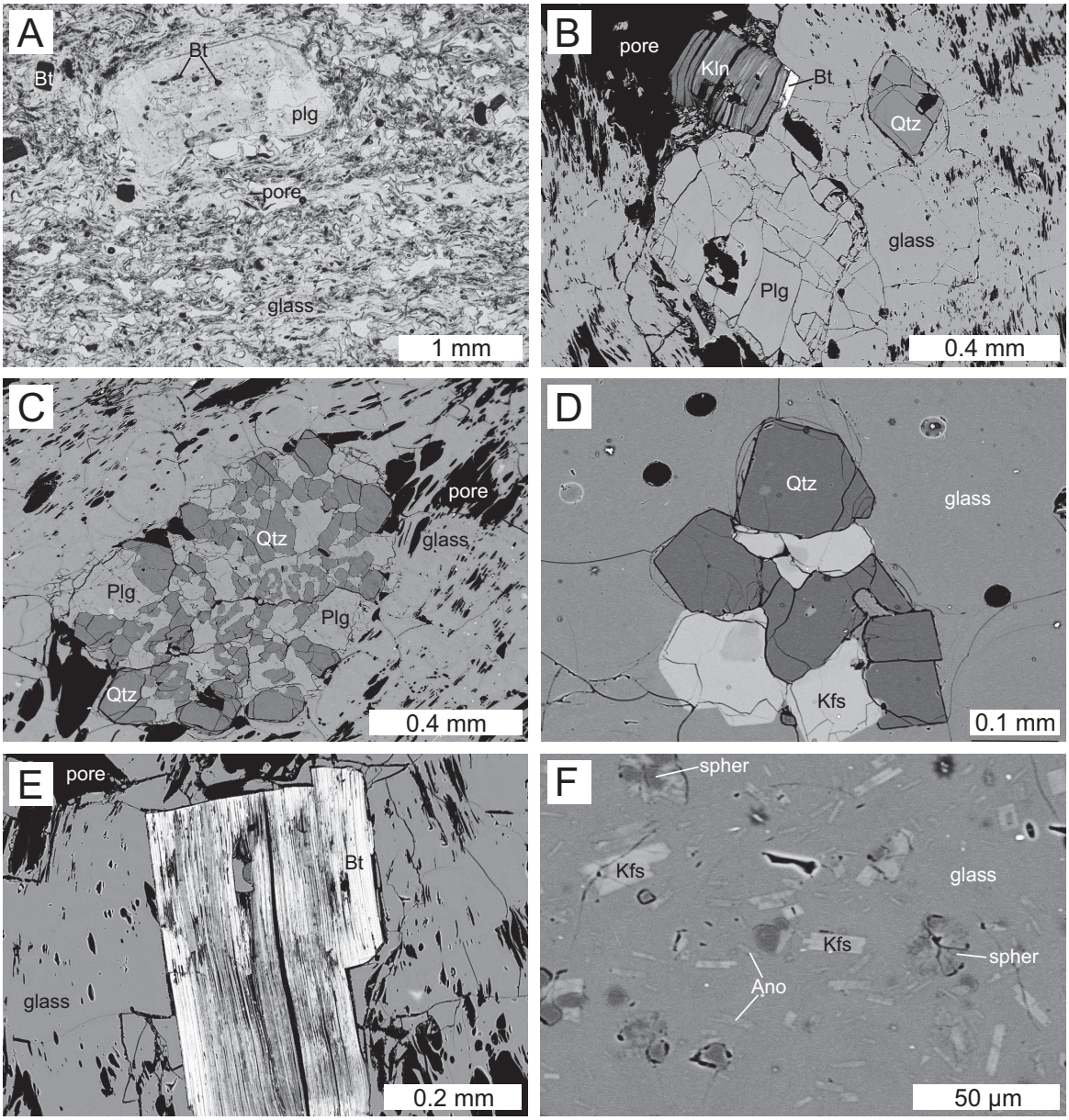

Fig. 9. Microphotograph (A) and BSE images (B–F) of perlites from the Jastrabá deposit: **A** — typical pale grey porous perlite with small biotite phenocrysts and a large plagioclase phenocryst with biotite and melt inclusions in the core (JS-24); **B** — plagioclase, biotite and quartz phenocrysts in a porous glass groundmass (JA-6); **C** — plagioclase and quartz aggregate in a porous glass groundmass (JS-22c); **D** — sanidine and quartz aggregate in a glassy groundmass (JA-6a); **E** — biotite phenocryst affected by kaolinization (JA-6); **F** — sanidine and anorthoclase microlites and small spherulites in a glassy groundmass (JA-6a).

pumiceous and moderately porous perlites (Fig. 10A, B) and (2) narrow stretched pores that either associate with open larger pores in moderately porous perlites showing flow banding (Fig. 10C, D) or represent sporadic pores in dense perlites (Fig. 10E, F). Textural relationships indicate that the larger open pores postdate the narrow-stretched ones – open pores deform and dismember the narrow-stretched ones (Figs. 8E and 10C). According to the 3D X-ray tomography, the porosity of perlites varies from almost zero in the dark dense ones up to 45 % in the pale grey pumiceous ones (Fig. 11). With the exception of the densest perlites, pores are mutually interconnected and perlites are permeable due to a network of interconnected pores (Varga et al. 2019).

Perlite phase composition (X-ray diffraction analysis)

Figures 12 and 13 show the results of X-ray diffraction (XRD) measurements on representative raw perlite samples. The obtained XRD patterns indicate mostly amorphous volcanic glass represented by a hump between 13° and 39° 2 Theta. The content of glass in perlites of the LPB deposit is 91.1–98.0 wt. %, in homogenous perlites of the JST deposit

94.5–97.1 wt. % (Fig. 12, Table 1, El. Suppl. 5). Rather low contents of biotite, plagioclase, alkali feldspar, cristobalite and quartz are documented by occasional XRD peaks in the diffraction patterns (Fig. 12). Differences in glass content and mineral composition among textural varieties of the LPB deposit are minimal (Table 1, El. Suppl. 5). The grey, porous variety of perlite shows a slightly higher content of glass if compared to dark varieties. Perlite with flow banding shows the same contents of glass and crystalline phases as the previous varieties. In perlites of the JST deposit the content of plagioclase is a little higher than the alkali feldspar content (Table 1, El. Suppl. 5). A small amount of kaolinite was sometimes observed too. A slightly lower amount of amorphous glass and higher amount crystalline phases, predominantly feldspars and partly kaolinite, were determined in the granular matrix of perlitic breccia (Fig. 13D, Table 1, El. Suppl. 5).

Zeolite and clay minerals, as products of glass alteration, were not distinguished or were very rare, in both deposits. Even macroscopically observed altered yellowish rock contains around 94 wt. % of glass (sample PL-134b in the El. Suppl. 3 and 5). A significant presence of smectite (almost 50 wt. %) was identified only in dark brown spots in the uppermost part of perlitic extrusive breccia in the western part of the LPB deposit (sample PL-141a,b in the El. Suppl. 3 and 5). Their colour is due to a small amount of goethite. The dark brown spots could be relicts of small fractures and/or channels

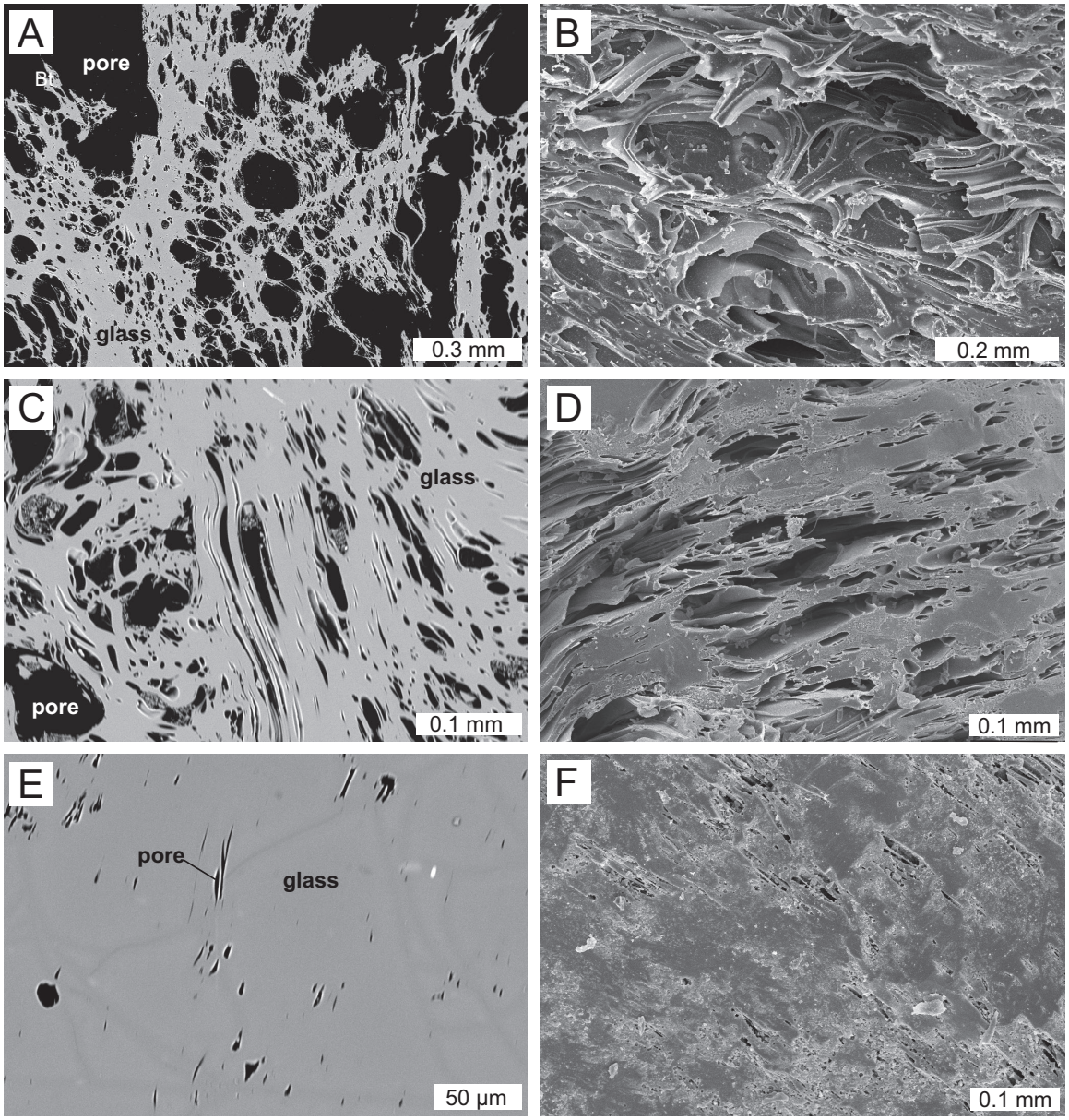

Fig. 10. BSE images (A, C, E) and SEM images (B, D, F) of porosity types in perlites of the Lehôtka pod Brehmi and Jastrabá perlite deposits: **A, B** — relatively large, open and less deformed pores of pale grey porous/pumiceous perlites (PL-22 and PL-4b); **C, D** — strongly deformed, stretched pores in less porous grey perlites showing flow banding (PL-10 and JS-25); **E, F** — sporadic narrow stretched pores in dark dense perlites (PL-6a). Note a network of darker bands in the BSE image E that indicates a higher degree of the hydration along incipient fractures.

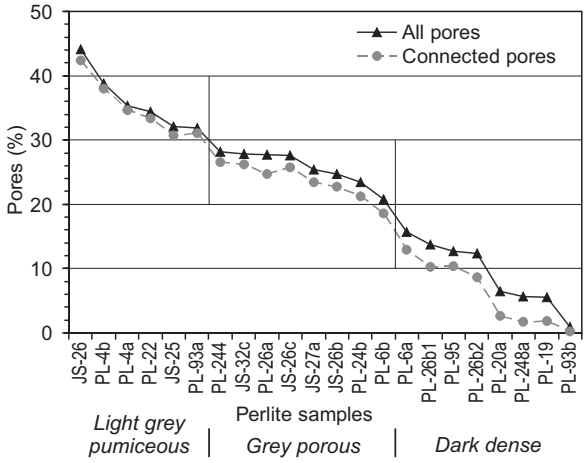

Fig. 11. Porosity of selected perlite samples from the Lehôtka pod Brehmi (PL) and Jastrabá (JS) deposits determined by X-ray computed microtomography. Connected pores represent those pores that are mutually interconnected for the distance of at least 4 mm. Data from Varga (2018).

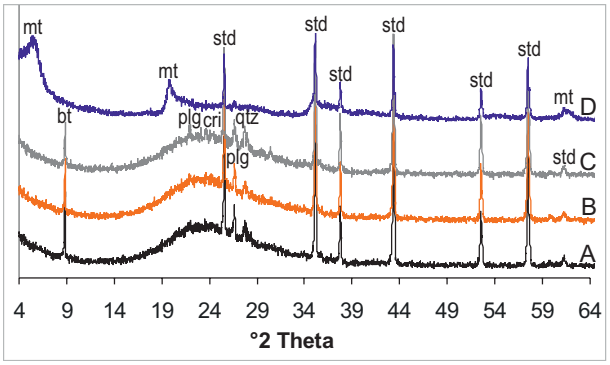

Fig. 12. XRD patterns of perlite from the Lehôtka pod Brehmi deposit (A, B, D) and Jastrabá deposits (C): **A** — dark dense variety (PL-140a); **B** — grey porous variety (PL-140b); **C** — grey porous variety (JS-22a); **D** — rare altered perlite (PL-141b); bt — biotite, cri — cristobalite, plg — plagioclase, qtz — quartz, mt — montmorillonite, std — Al_2O_3 as internal standard.

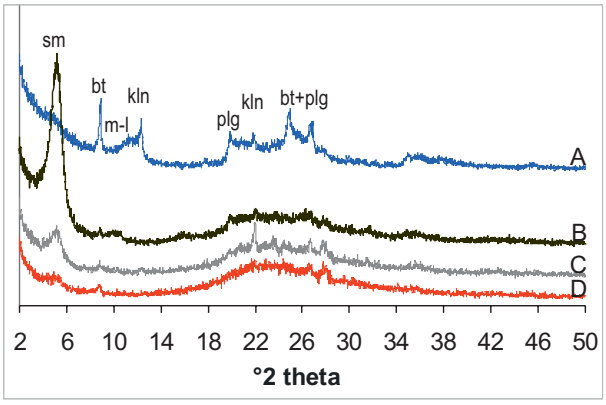

Fig. 13. XRD oriented patterns of clay fractions from the Lehôtka pod Brehmi deposit (**A–C**; PL-248, PL-151c, PL-140d) and Jastrabá deposit (**D**; JS-26a) after saturation by ethylene glycol. sm — smectite, bt — biotite, m-l — mixed-layered clay mineral, kln — kaolinite, plg — plagioclase.

that allowed hydrothermal fluids to migrate through the perlite breccia pile.

Trace amounts of smectite, however, were determined in clay fractions of pale porous and dark dense perlites of the LPB deposit. We estimate that the smectite content is less than 0.5 wt. % in bulk perlite fragments based on the proportion of clay fraction after milling (less than 7 wt. %) and determination of smectite amount by semi quantitative XRD analyses of clay fraction (less than 5 wt. %, Fig. 13A). Such a small amount of smectite is below the detection limit of bulk rock XRD analysis. A slightly higher amount of smectite was detected in the clay fraction of the LPB deposit perlite breccia granular matrix (Fig. 13B, C). Only a single sample of granular matrix (PL-140d) contained a detectable amount of smectite (2.6 wt. %) in bulk rock (Table 1, El. Suppl. 5). Kaolinite was identified in some clay fractions of samples from the LPB deposit but its amount is even lower compared to smectite (Fig. 13).

Glassy rhyolite and pumiceous tuffs underlying the western side of the Jastraba volcano (Fig. 3) are altered to zeolites (clinoptilolite and mordenite) and to opal-C or opal-CT (Table 1, El. Suppl. 5). Kraus et al. (1994) assigned this alteration to diagenesis and hydrothermal processes driven by cooling rhyolite cryptodomes.

Chemical composition of perlites and perlite glasses

At the time of eruption in the low-pressure environment the water content of the rhyolite lava was negligible, just a few tenths of percent (Ross & Smith 1955; Uhlík et al. 2015; Selingman et al. 2016). So, here we shall discuss analyses recalculated to the dry basis to eliminate the influence of the secondary hydration on concentrations of analysed elements. Original whole-rock chemical analyses and microprobe glass analyses as well as analyses recalculated to the dry basis are presented in the El. Suppl. 6 and 7. While whole rock analyses represent homogenized samples of the volume around 200 cm^3, including glassy groundmass, phenocrysts, accessory minerals and microlites, microprobe analyses represent a spot 10 μm in diameter in pure glass. It is important to remember this aspect when comparing the results of both types of analysis and their dispersion patterns. Compositions of perlites and their glass are characterized by statistical parameters in the Tables 2 and 3, by a set of plots in the Figures 14–16 and by additional plots in the El. Suppl. 8.

The chemical composition of perlites confirms their petrographic classification as rhyolites. In the total alkalis/silica (TAS) plot perlites as well as their glass fall fully in the field of rhyolites (Fig. 14) and are clearly separated from the field of andesites and dacites of the Central Slovakia Volcanic Field. Perlite compositions from different lithological units of the LPB deposit mutually overlap and show in this plot a different position than perlites of the JST deposit. However, perlites of both deposits overlap with projection points of the Jastrabá Fm. rhyolites that show a higher overall variability. Considering differences in chemical composition of perlites

Table 1: The results of X-Ray powder diffraction quantitative analyses (wt. %) of various types of perlite from the Lehôtka pod Brehmi and Jastrabá deposits. Results of individual analyses are given in the El. Suppl. 5.

	Lehôtka pod Brehmi deposit																					
	Grey porous perlites					Fine grained matrix					Dark dense perlites					Flow banded perlites					Altered perlites				
	N	n	Max	Min	Avg.	N	n	Max	Min	Avg.	N	n	Max	Min	Avg.	N	n	Max	Min	Avg.	N	n	Max	Min	Avg.
Quartz	13	12	1.6	0.2	0.9	6	6	1.3	0.4	0.8	12	11	1.6	0.0	1.1	3	2	1.1	0.0	0.4	3	2	0.6	0.0	0.3
K-feldspar	13	13	1.9	0.0	0.6	6	5	1.8	0.0	0.6	12	10	3.1	0.0	1.0	3	2	1.0	0.0	0.3	3	0	0.0	0.0	0.0
Plagioclase	13	4	4.4	0.4	2.2	6	6	6.3	2.4	4.2	12	12	7.8	1.0	3.2	3	2	3.2	1.0	1.4	3	2	3.9	0.0	1.4
Pyroxene	13	0	0.0	0.0	0.0	6	0	0.0	0.0	0.0	12	1	0.3	0.0	0.0	3	2	0.0	0.0	0.0	3	1	0.5	0.0	0.2
Goethite	13	0	0.0	0.0	0.0	6	0	0.0	0.0	0.0	12	0	0.0	0.0	0.0	3	2	0.0	0.0	0.0	3	2	2.7	0.0	1.2
Rutile	13	1	0.2	0.1	0.1	6	1	0.1	0.0	0.0	12	8	0.2	0.0	0.1	3	2	0.1	0.0	0.0	3	0	0.0	0.0	0.0
Biotite	13	10	1.7	0.0	0.8	6	6	1.6	0.7	1.2	12	11	3.0	6.0	1.0	3	2	6.0	1.0	2.3	3	3	3.2	1.0	2.1
Kaolinite	13	1	0.1	0.1	0.1	6	1	0.4	0.0	0.1	12	0	0.0	0.0	0.0	3	2	0.0	0.0	0.0	3	2	3.5	0.0	1.5
Smectite	13	0	0.0	0.0	0.0	6	1	2.6	0.0	0.4	12	0	0.0	0.0	0.0	3	2	0.0	0.0	0.0	3	2	47.0	0.0	27.1
Opal-C/CT	13	0	0.0	0.0	0.0	6	0	0.0	0.0	0.0	12	0	0.0	0.0	0.0	3	2	0.0	0.0	0.0	3	2	10.5	0.0	4.1
Cristobalite	13	13	0.7	0.1	0.2	6	6	0.7	0.3	0.5	12	8	0.6	0.0	0.2	3	2	0.2	0.0	0.1	3	1	0.4	0.0	0.1
Glass	13	13	98.0	92.4	95.3	6	6	95.4	87.2	92.2	12	12	96.6	85.4	93.4	3	2	93.4	85.4	59.6	3	3	94.1	43.8	62.0

	Jastrabá perlite deposit																			
	Grey porous perlites					Fine grained matrix					Pyroclastic flow deposits					Altered underlying rocks				
	N	n	Max	Min	Avg.	N	n	Max	Min	Avg.	N	n	Max	Min	Avg.	N	n	Max	Min	Avg.
Quartz	10	10	1.8	0.3	0.9	3	3	1.5	1.1	1.3	4	4	1.7	0.6	1.0	5	1	0.3	0.0	0.1
K-feldspar	10	10	1.8	0.1	0.9	3	3	3.0	1.5	2.1	4	4	9.0	1.9	6.8	5	5	24.2	2.3	11.5
Plagioclase	10	9	2.7	0.0	1.7	3	3	4.0	3.0	3.4	4	4	6.0	1.0	3.0	5	3	5.5	0.0	1.8
Rutile	10	0	0.0	0.0	0.0	3	1	0.1	0.0	0.0	4	0	0.0	0.0	0.0	5	2	0.1	0.0	0.0
Kaolinite	10	2	1.1	0.0	0.2	3	3	3.7	0.2	1.4	4	2	3.8	0.0	1.4	5	1	2.1	0.0	0.4
Biotite	10	5	0.4	0.0	0.2	3	3	0.9	0.3	0.6	4	3	0.6	0.0	0.3	5	3	0.8	0.0	0.2
Cristobalite	10	8	0.6	0.0	0.3	3	1	0.4	0.4	0.1	4	4	4.1	0.4	2.0	5	4	4.9	0.0	2.6
Glass	10	10	97.1	94.5	95.8	3	3	93.4	87.3	91.0	4	4	95.8	75.5	85.6	5	5	67.1	2.0	30.8
Smectite	10	0	0.0	0.0	0.0	3	0	0.0	0.0	0.0	4	0	0.0	0.0	0.0	5	1	1.5	0.0	0.3
Illite	10	0	0.0	0.0	0.0	3	0	0.0	0.0	0.0	4	0	0.0	0.0	0.0	5	3	13.6	0.0	4.4
Mordenite	10	0	0.0	0.0	0.0	3	0	0.0	0.0	0.0	4	0	0.0	0.0	0.0	5	3	50.3	0.0	14.2
Opal-CT	10	0	0.0	0.0	0.0	3	0	0.0	0.0	0.0	4	0	0.0	0.0	0.0	5	5	30.6	8.9	21.1
Clinoptilolite	10	0	0.0	0.0	0.0	3	0	0.0	0.0	0.0	4	0	0.0	0.0	0.0	5	4	60.4	0.0	12.5

N — number of analyzed samples, n — number of analyzes with a given phase, Max — maximum quantity of the phase, Min — minimum quantity of the phase, Avg. — arithmetic average of the phase

Table 2: Statistical parameters of whole rock major element composition of perlites from the Lehôtka pod Brehmi and Jastrabá deposits (wt. % recalculated to 100 % dry, individual original analyses are given in the El. Suppl. 6).

Oxide	SiO_2	TiO_2	Al_2O_3	Fe ox	MnO	MgO	CaO	Na_2O	K_2O	H_2O*
Lehôtka pod Brehmi deposit										
Number	51	51	51	51	51	51	51	51	51	51
Minimum	72.81	0.135	13.37	1.329	0.041	0.197	1.169	2.24	4.83	3.00
Maximum	75.14	0.333	14.37	3.065	0.094	0.468	1.815	3.08	5.93	4.90
Median	74.15	0.213	13.75	1.809	0.042	0.332	1.425	2.52	5.64	3.60
Average	74.13	0.215	13.76	1.874	0.047	0.337	1.418	2.54	5.62	3.72
Std. deviation	0.55	0.035	0.21	0.332	0.012	0.069	0.136	0.18	0.20	0.44
Jastrabá deposit										
Number	22	22	22	22	22	22	22	22	22	22
Minimum	73.84	0.083	13.10	1.230	0.042	0.104	0.951	1.81	4.99	3.60
Maximum	76.95	0.249	15.29	1.812	0.074	0.385	1.486	2.95	5.73	6.00
Median	76.31	0.085	13.46	1.390	0.063	0.137	0.989	2.03	5.41	5.20
Average	76.13	0.101	13.61	1.434	0.061	0.159	1.020	2.08	5.38	5.15
Std. deviation	0.73	0.037	0.49	0.160	0.007	0.059	0.115	0.25	0.17	0.58

* water content = LOI, presence of other constituents in the LOI is negligible

from both deposits (Table 2, Figs. 14 and 15, El. Suppl. 6 and 8), perlites from the JST deposit are relatively enriched in silica and incompatible elements Ba, Nb, Th, U, light REE and relatively impoverished in all other analysed elements. Naturally, this is reflected in the relationship of element concentrations with increasing silica content – concentrations of the above-mentioned incompatible elements increase (e.g. Nb, Fig. 15F) while concentrations of the most compatible elements decrease (e.g. Na, K and Fe, Fig. 15A, B, D). A differentiation trend has been observed only in the case of Al, Ca, Fe, Mg and Ti

Table 3: Statistical parameters of glass major element composition in perlites from the Lehôtka pod Brehmi and Jastrabá deposits by EMPA (wt. % recalculated to 100 % dry except for the assumed water content, individual original analyses are in the El. Suppl. 7).

Oxide	SiO_2	TiO_2	Al_2O_3	Fe ox	MnO	MgO	CaO	Na_2O	K_2O	H_2O*
Lehôtka pod Brehmi deposit, dark dense perlites										
Number	138	135	138	137	138	138	138	138	138	138
Minimum	75.46	0.064	12.15	0.390	0.000	0.000	0.411	1.01	3.55	1.59
Maximum	78.99	0.227	13.36	1.568	0.139	0.158	1.136	4.05	6.94	7.33
Median	76.76	0.113	12.77	0.962	0.044	0.064	1.012	2.61	5.61	4.02
Average	76.81	0.113	12.78	0.929	0.045	0.065	0.996	2.56	5.59	3.87
Std. deviation	0.55	0.023	0.24	0.250	0.027	0.036	0.099	0.44	0.53	1.10
Lehôtka pod Brehmi deposit, grey porous perlites										
Number	100	100	100	100	100	100	100	100	100	100
Minimum	75.36	0.048	11.84	0.542	0.000	0.000	0.77	1.38	4.89	1.53
Maximum	78.23	0.159	13.30	1.382	0.100	0.144	1.14	4.76	6.53	6.19
Median	76.50	0.110	12.70	1.125	0.044	0.075	1.02	2.64	5.66	4.18
Average	76.56	0.111	12.69	1.093	0.044	0.069	1.01	2.67	5.63	3.01
Std. deviation	0.51	0.019	0.28	0.137	0.025	0.035	0.07	0.51	0.43	0.93
Jastrabá deposit perlites										
Number	78	78	78	78	78	78	78	78	78	78
Minimum	76.39	0.003	11.84	0.226	0.000	0.000	0.198	0.77	4.63	2.76
Maximum	79.54	0.140	12.96	1.177	0.154	0.168	1.079	3.71	6.49	7.38
Median	78.06	0.045	12.42	0.933	0.068	0.032	0.787	2.55	5.05	4.73
Average	78.07	0.051	12.42	0.903	0.068	0.036	0.768	2.38	5.16	4.87
Std. deviation	0.73	0.026	0.24	0.151	0.030	0.035	0.153	0.65	0.39	1.02

* water content = 100 % minus sum of oxides in the original microprobe analysis

(Fig. 15D, El. Suppl. 8). However, in the case of Fe, Mg and Al the observed trends for perlites of individual deposits do not correspond to differences among perlites of both deposits.

The projection points of pure glass are shifted generally towards silica enriched compositions (Figs. 14, 15). On average, glass in perlites of the LPB deposit is 2.5 % richer in silica as corresponding perlites and glass in perlites of the JST deposit is 1.9 % richer in silica than corresponding perlites (Tables 2 and 3). Average concentrations of alkalis in glass and corresponding perlites are almost equal, while average concentrations of Al, Ca, Fe, Mg and Ti in glass are lower than in corresponding perlites. The TAS plot in the Fig. 14 and the plots A, B and D in the Fig. 15 demonstrate that concentrations of all elements in glass generally decrease with the increasing silica content. The compositional shift among perlites and their glass is different from the compositional shift between perlites of the LPB and JST deposits.

EPMA spot analyses of pure glass compositions show much higher dispersion than corresponding homogenized whole rock perlite compositions, especially in the case of Na_2O and K_2O (Fig. 15A, B). However, the dispersion of glass compositions in the TAS plot (Fig. 14) is smaller. The plot E (K_2O vs. SiO_2) in the Figure 15 shows data for grey porous perlites of the LPB deposit and their glass distinguished according to individual samples. The plot demonstrates that the high dispersion of K_2O contents can be only partially attributed to differences among samples, while a variability of K_2O contents among analyses from individual samples dominates.

Plots in the Figure 16 show a general absence of relationships between water content and concentrations of SiO_2 and K_2O in perlites and their glass, while Na_2O shows a general negative correlation (analyses were recalculated to 100 % dry to avoid the influence of the water content). No relationships have been observed also in the case of other major oxides apart from the generally higher water content in perlites of the JST deposit (El. Suppl. 8). Plots for silica and alkalis in the Figure 16 are dominantly influenced by compositional differences among perlites of the LPB and JST deposits. Projection points of glass compositions from individual deposits show a high variability of water content without any relationship with K_2O content, only a very weak positive correlation with SiO_2 content and a more pronounced negative correlation with Na_2O content that is reflected also in a weak positive correlation with the K_2O/Na_2O ratio.

Water in perlite – loss on ignition (LOI)

Mass spectroscopy accompanied by simultaneous heating has confirmed that the dominant volatile species of studied perlites is water (Pálková et al. 2020). Therefore, it is possible to consider LOI data as a water release. In perlites from the LPB deposit the water content is 4.0 wt. % on average (Table 4, El. Suppl. 9). Despite the subdivision of the data from the deposit into western and eastern parts, the water content of perlites is homogeneous, including perlite fragments of phreatomagmatic pyroclastic rocks (Table 4). Only small differences in water content, 0.5 wt. % on average, were observed between grey porous and dark dense perlites. Similar values were also measured in perlites from Szabóova skala (Table 4). The granular perlitic breccia matrix shows the highest water content in the LPB deposit (4.8 wt. % on av., Table 4). Fine perlite grains have a larger surface area that enables

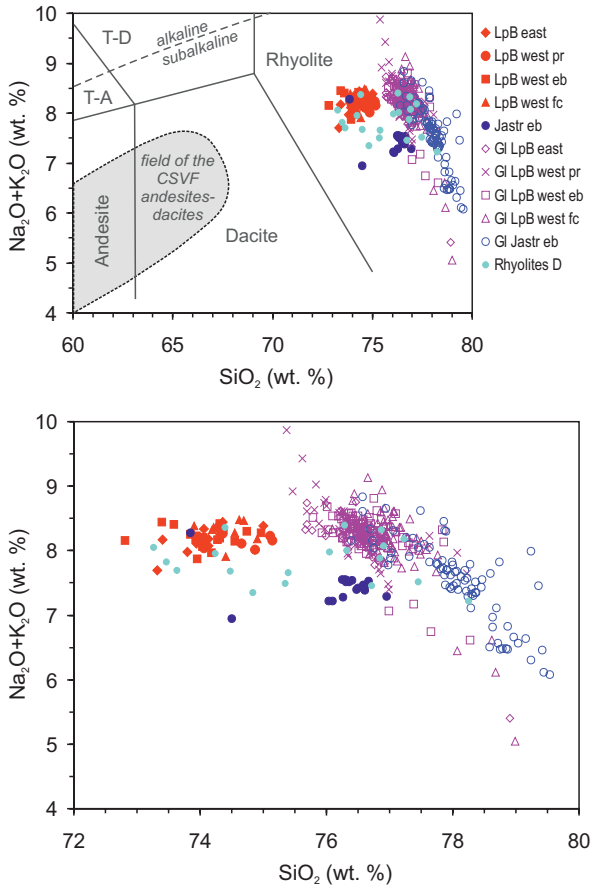

Fig.14. Plot total alkalis vs. SiO_2 (TAS) for analyses of perlites from the Lehôtka pod Brehmi and Jastrabá deposits, their glass and associated rhyolites of the Jastrabá Fm. Analyses recalculated to 100 % dry are in the El. Suppl. 6 and 7, rhyolite analyses are from the work of Demko et al. (2010). Rock fields are according to Le Bas (1986), T-A and T-D are fields of trachyandesites and trachydacites, respectively. The composition of Central Slovakia Volcanic Field andesites–dacites is from Lexa et al. (1997). Data are in the legend distinguished according to lithological units: *LpB* stands for Lehôtka pod Brehmi, *Jastr* for Jastrabá, *west* and *east* for western and eastern parts of the LpB deposit, *pr* for pyroclastic rocks, *eb* for extrusive breccia, *fc* for lava flows and cryptodomes. Data points with the prefix *Gl* represent glass compositions by EMPA. The lower plot represents an enlargement of the rhyolite field in the upper plot.

an increased water adsorption (Varga et al. 2019). The presence of higher amount of loosely bound water in fine grained matrix compared to perlite fragments and blocks was confirmed by a higher release of water upon drying at 105 °C (1.4 vs. 0.3–0.5 wt. % on av., Table 4). Notable water content, almost 15 wt. % on average, was determined in few altered samples, where the occurrence of clay minerals, predominantly smectites (Table 1), corresponds to the presence of more than 50 % of the loosely bound water in altered samples (Table 4, El. Suppl. 9).

Perlites from the JST deposit show a higher water content than perlites from the LPB deposit, 5 wt. % on average (Table 4, El. Suppl. 9). About 10 % of their total water content was released at 105 °C, similarly as in the case of perlites from the LPB deposit. Samples from the upper part of the deposit (just beneath the overburden) and samples taken from debris show slightly increased water contents. Owing to loosely bound water the granular matrix of perlitic breccia shows a slightly higher water content if compared with perlite of breccia fragments at the same site. Perlites of the JST deposit are not affected by alteration with the exception of a small amount of kaolinite in some samples (Table 1), associated with an increased total water content. Significantly higher water contents were observed in samples from greenish altered glass and tuffs underlying the Jastrabá volcano at the west that contain zeolites (Table 1). The total water loss of the zeolite-bearing sample with opal-CT (JS-42, El. Suppl. 5) was 9.9 wt. %, while 5 wt. % of loosely bound water was already removed after drying (El. Suppl. 9).

Discussion

The complex characteristics of perlites require consideration of various aspects starting with the geology of deposits and their evolution through petrological, mineralogical and compositional aspects, role of porosity and water content and its nature in perlite. Naturally, we shall also consider how these aspects contribute to understanding of the perlite's origin and its utilization.

Geology and evolution of the Lehôtka pod Brehmi and Jastrabá perlite deposits

The creation of a perlite deposit needs a coincidence of four essential factors (modified after Barker & Santini 2006): (1) a silicic magmatic/volcanic activity of phenocryst poor magma; (2) vesiculation, dehydration, rapid cooling and fracturing leading to accumulation of a large enough volume of glassy breccia; (3) conditions that allow for a subsequent secondary hydration of glass; (4) preservation. In the Central Slovakia Volcanic Field (CSVF) only two of the numerous occurrences are voluminous enough to represent exploitable perlite deposits.

The Lehôtka pod Brehmi perlite deposit

The monogenetic rhyolite volcano, hosting the Lehôtka pod Brehmi perlite deposit, evolved above a thick succession of sedimentary rocks filling the Žiar basin, including groundwater-bearing gravel and sand horizons (Konečný et al. 2003). Thus, the magma rising along one of the marginal faults of the basin met groundwater and further evolution of the volcano was more or less governed by the water–magma interaction. Contact of hot magma with water or wet sediment causes its immediate quenching (transformation of viscous melt into glass) and contraction fracturing giving rise to glassy angular fragments and shards – hyaloclastite (e.g., Pichler 1965; Cas & Wright 1987; Scutter et al. 1998; Van Otterloo et al. 2015). At the same time fracturing enables explosive molten-fuel

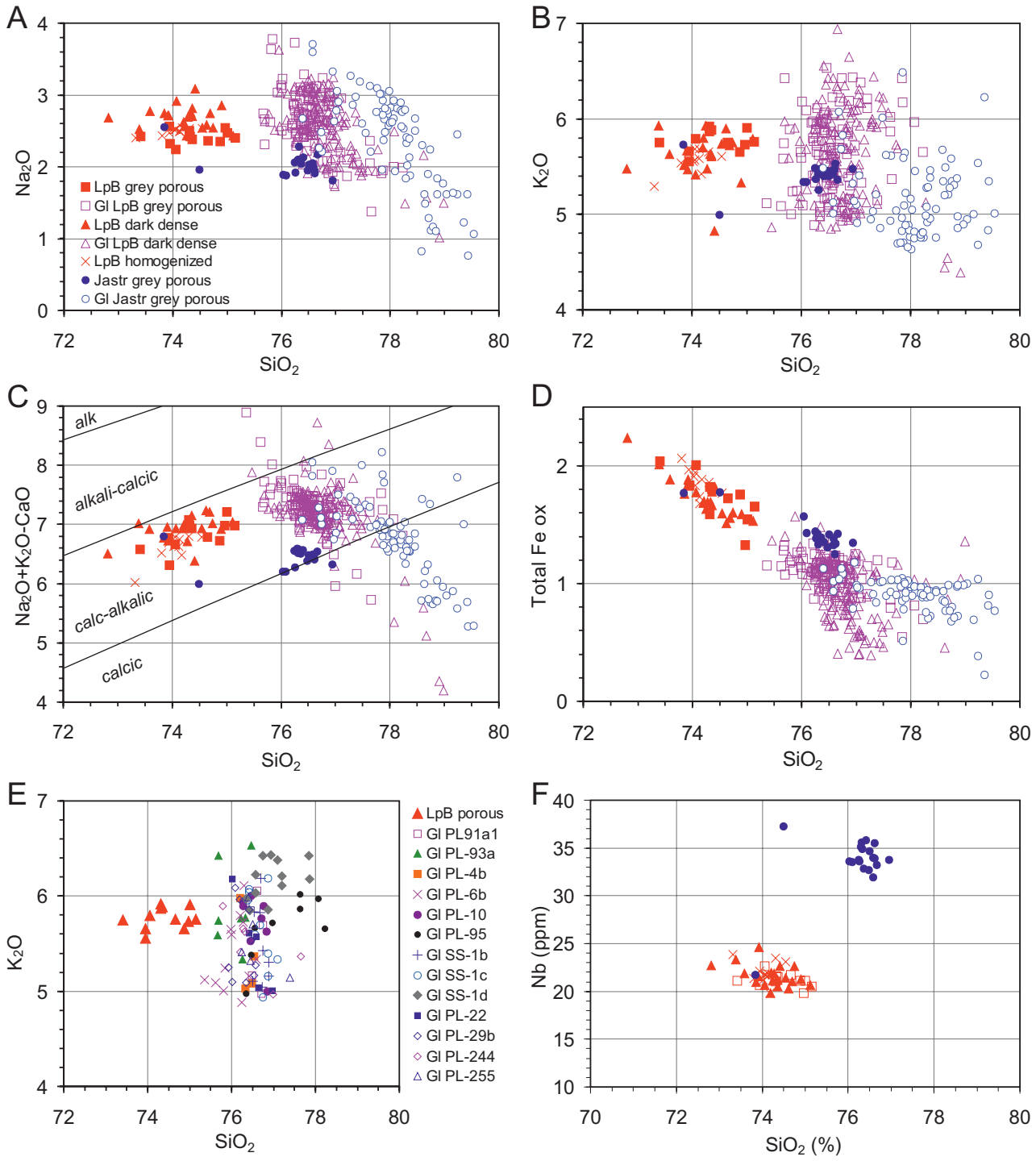

Fig. 15. Plots of perlite and perlite glass compositions recalculated to 100 % dry for the Lehôtka pod Brehmi and Jastrabá deposits. Original and recalculated analyses are in the El. Suppl. 6 and 7. Data are distinguished according to the perlite type. *LpB* stands for Lehôtka pod Brehmi, *Jastr* for Jastrabá, data points with the prefix *Gl* represent glass compositions, *homogenized* for samples of extrusive breccia obtained from core-less drilling. Legend in the plot A applies also to the plots B–D and F. The plot E shows compositions of grey porous perlites of the Lehôtka pod Brehmi deposit (LpB porous) and their glass compositions distinguished according to individual samples. Fields of alkalic, alkali-calcic, calc-alkalic and calcic rocks in the plot C are based on the modified alkali-lime index (MALI) by Frost et al. (2001).

coolant interaction (Austin-Erickson et al. 2008) and water or its part is turned into steam. A further destiny of the hyaloclastite material depends on the effective water/magma ratio (cf. Wohletz & Sheridan 1983). At a relatively low water/magma ratio all water is turned into steam and the expanding steam generates a phreatomagmatic explosion. The heat energy of the magma is effectively transferred into a mechanical energy that drives the explosion (Cas & Wright 1987). At a relatively

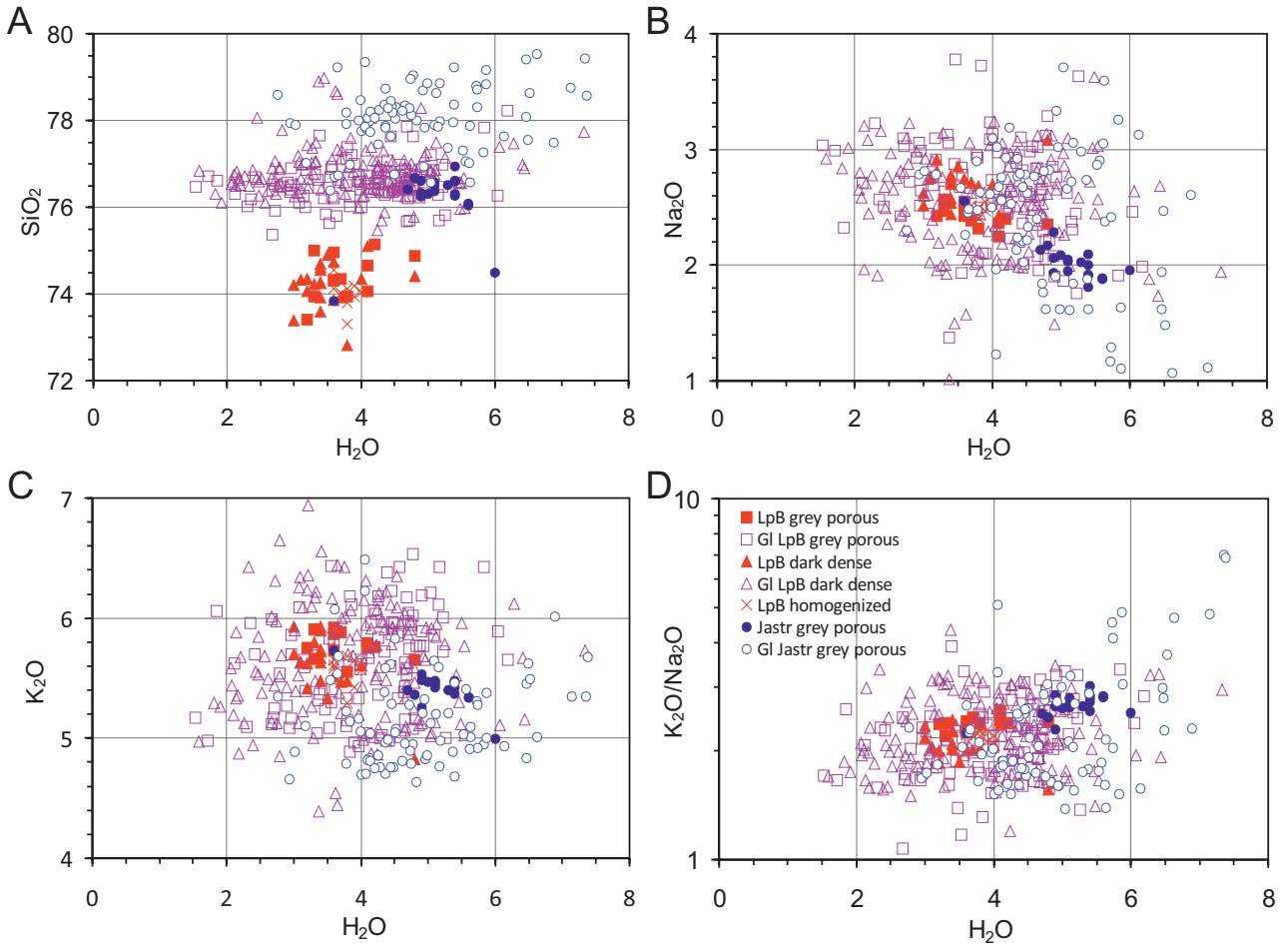

Fig. 16. Plots of silica and alkalis recalculated to 100 % dry vs. water content for perlites and perlite glass of the Lehôtka pod Brehmi and Jastrabá deposits. Original and recalculated analyses are in the El. Suppl. 6 and 7. Data are distinguished according to the perlite type. *LpB* stands for Lehôtka pod Brehmi, *Jastr* for Jastrabá, data points with the prefix *Gl* represent glass compositions, *homogenized* for samples of extrusive breccia obtained from core-less drilling. Legend in the plot D applies also to other plots.

Table 4: Summarized data of loss on ignition (LOI, 950 °C) and loss on drying (105 °C) of perlites and surrounding rocks (wt. %) from the Lehôtka pod Brehmi deposit, Szabóova skala and the Jastrabá deposit. Results of individual analyses are given in the El. Suppl. 9.

	Position/variety	number	950 °C				105 °C				Difference (950–105 °C)	% 105 °C
			AM	SD	Max	Min	AM	SD	Max	Min		
Lehôtka pod Brehmi	Phreatomagmatic pyroclastic rocks	8	4.3	0.2	4.6	3.8	0.4	0.1	0.5	0.2	3.9	8.8
	Western part of the deposit	32	4.0	0.9	7.5	3.2	0.6	0.7	3.9	0.1	3.4	14.0
	Eastern part of the deposit	19	3.9	0.7	5.4	3.1	0.7	0.5	1.9	0.2	3.2	15.8
	Dark dense type	17	3.5	0.3	4.3	3.1	0.3	0.1	0.5	0.1	3.2	8.0
	Grey porous type	28	3.9	0.5	5.1	3.2	0.5	0.2	1.3	0.2	3.4	11.6
	Granular matrix	13	4.8	1.1	7.5	3.8	1.3	0.9	3.9	0.5	3.5	25.7
	Total	62	4.5	2.9	22	3.1	1.0	2.3	14.5	0.1	3.5	15.8
	Altered perlite	3	14.8	7.5	22	4.5	9.2	5.8	14.5	1.1	5.6	52.4
Szabóova skala	Dark dense type	4	3.5	0.1	3.7	3.3	0.2	0.1	0.4	0.1	3.3	6.3
	Grey porous type	2	4.0	0.2	4.1	3.8	0.5	0.2	0.6	0.3	3.5	11.2
	Total	6	3.7	0.3	4.1	3.3	0.3	0.2	0.6	0.1	3.4	7.9
Jastrabá	Grey porous type	17	4.9	0.7	5.4	3.4	0.4	0.1	0.7	0.2	4.5	8.4
	Granular matrix	10	5.5	0.7	7.0	4.4	0.6	0.3	1.3	0.3	4.6	11.5
	Total	27	5.1	0.6	7.0	3.4	0.5	0.2	1.3	0.2	4.6	9.6
	Surrounding pyroclastic flow deposits	7	4.2	1.3	5.7	1.4	0.7	0.4	1.5	0.4	3.5	18.9
	Underlying altered rocks	2	8.1	1.8	9.9	6.3	4.2	0.8	5.0	3.4	3.9	52.2

AM — arithmetic mean, SD — standard deviation, Max — maximum value, Min — minimum value, % 105 °C — proportion of weight loss after drying at 105 °C from the total weight loss on LOI.

high or a very low water/magma ratio, not enough steam can be formed to initiate an explosive event and further evolution of the hyaloclastite material is un-explosive.

Remnants of the LPB rhyolite volcano represent products of two closely situated volcanic centres that were active in a succession (Fig. 2). As there is no difference in their petrographic and chemical composition (see the petrographic description above and Fig. 14) they are considered comagmatic. The activity started with violent phreatomagmatic eruptions at the eastern volcanic centre. The corresponding horizon of tuffs is known only from prospection boreholes and we lack a detailed lithological description. However, the phreatomagmatic type of eruptions is confirmed by the dominantly angular form of glass fragments and by a significant admixture of mostly andesite pebbles and sand grains (Beňo & Očenáš 1962) coming from gravel and sand deposits of the relevant aquifer – the site of the phreatomagmatic explosions. Subsequent extrusion of coarse hyaloclastite breccias forming the eastern part of the deposit (Figs. S1–S4 in the El. Suppl. 2) implies a significant change in the water/magma ratio. Quench fragmentation giving rise to the hyaloclastite breccia is confirmed by the angular and polygonal shapes of fragments with curviplanar edges, presence of chilled blocks showing radial joints, a low proportion of matrix and locally observed jig-saw pattern grading into coherent lava tongues (cf. McPhie et al. 1993; Németh et al. 2008).

Extrusion of hyaloclastite breccias ended the activity in the eastern volcanic centre and further activity moved to the western volcanic centre, where it was again initiated by phreatomagmatic eruptions that gave rise to a tuff ring (section in the Fig. 2, Fig. 17A) and a related maar depression. A large proportion of explosive breccias implies a proximity to the volcanic centre that was situated south of the exposed part of the ring in the quarry. Alternation of explosive breccias with tuffs (Figs. S7–S10 in the El. Suppl. 2) points to a variable degree of fragmentation, reflecting temporal changes in the water/magma ratio (Wohletz & Heiken 1992; Van Otterloo et al. 2015). While textures of the tuffs (see the lithological description in the El. Suppl. 2) indicate a deposition dominantly by dry pyroclastic surges with subordinate fall that are

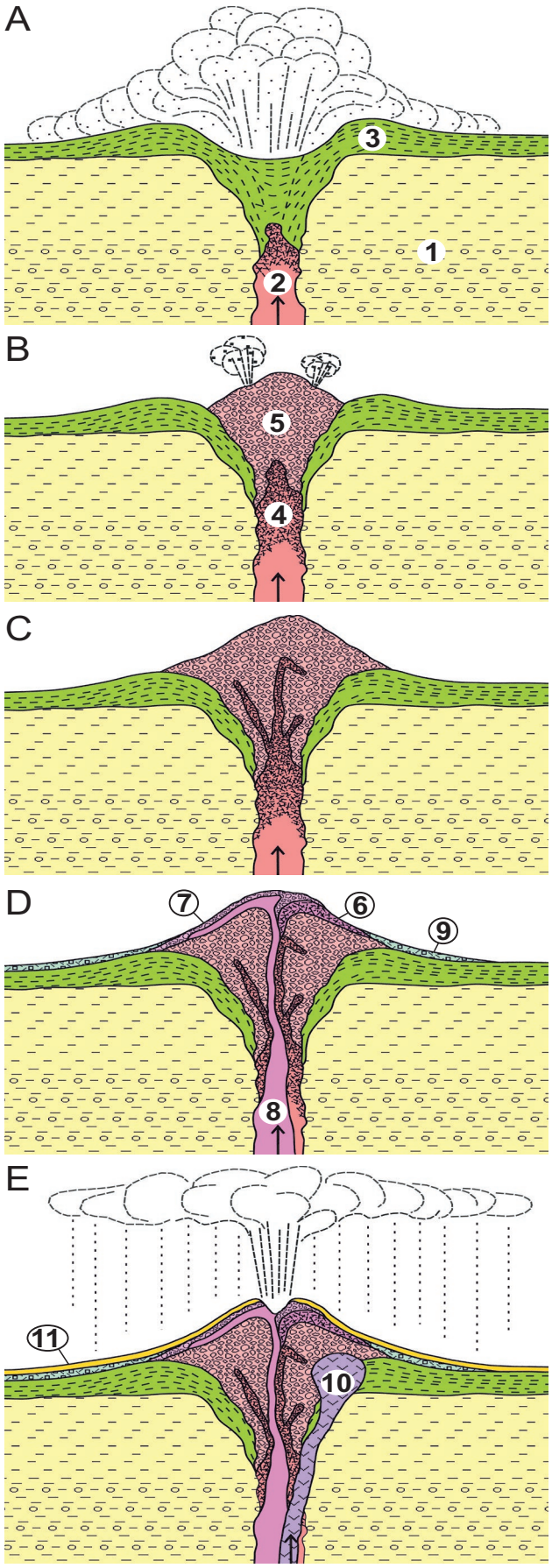

Fig. 17. A scheme of volcanic evolution at the western centre of the monogenentic rhyolite volcano hosting the perlite deposit Lehôtka pod Brehmi: **A** — initial phreatomagmatic eruptions at the contact of rising lava (2) with groundwater in aquifer of underlying sedimentary rocks (1) giving rise to a tephra ring (3) and related maar; **B**, **C** — further water/magma interaction caused a quench fragmentation of lava (4) and formation of hyaloclastite breccia (5) that was extruded to the surface forming a "dome"; **D** — diminishing water/magma interaction and a lesser extent of quench fragmentation resulted in the emplacement of a brecciated lava flow (6), associated hyaloclastite breccia (7) and a flow of coherent lava (8); reworking of loose material from the surface of the "dome" gave rise to aprons of epiclastic volcanic breccias next to the "dome" (9); **E** — activity of the volcano continued by the emplacement of two cryptodomes (10) and the final vulcanian/phreatic type of explosions that covered the volcano with a mantle of fine tephra (11).

characteristic for violent phreatomagmatic explosions, textures of the breccias point to deposition of a lower energy tephra jets material variably by the fall, flow and/or surge type mechanism (cf. Wohletz & Sheridan 1983; White & Houghton 2000).

The phreatomagmatic explosive activity was followed by an extrusion of the hyaloclastite-type breccias forming a dome-like pile filling the maar (section in the Fig. 2, Fig. 17B, C; Figs. S11–S14 in the El. Suppl. 2). Hyaloclastite breccias usually associate with subaqueous/submarine lava flows and extrusive domes, where they form at contact of lava and water (e.g., Pichler 1965; Cas & Wright 1988; Scutter et al. 1998). However, this was not the case of the LPB volcano as the underlying phreatomagmatic pyroclastic rocks reveal a terrestrial environment. The same types of angular and polygonal glass fragments in phreatomagmatic explosive breccias and overlying extruded hyaloclastite breccias imply a common origin of the hyaloclastite material. Apparently, the quench fragmentation took place at the contact of a rising magma with groundwater and the resulting hyaloclastite breccia was pushed subsequently to the surface. During the process of extrusion, most of the hyaloclastite breccia was mixed up on its own and became chaotic. Only small domains of the breccia show a preserved original "jig saw" pattern. The locally observed incipient stratification resulted from a mass wasting on steep slopes of the growing breccia pile ("dome").

The extrusion of the mixed hyaloclastite breccias was followed by an extrusion of coherent lava affected by quench fragmentation, passing upward into a hyaloclastite breccia (section in the Fig. 2, Fig.17D, Figs. S17–S18 in the El. Suppl. 2). Apparently, at this stage the extent of the water/magma interaction decreased and the coherent parts of the lava avoided a direct contact with water. The "dome" growth changed from endogenous to exogenous as indicated by lava flows and new portions of hyaloclastite breccia resting on slopes of the "dome" (cf. Williams 1932; Fink et al. 1990). One of the flows dominated by coherent lava is only 5–6 m thick and at least 200 m long (Fig. S15 in the El. Suppl. 2). The formation of such a flow requires a relatively low viscosity and yield strength (Fink & Griffiths 1998). In the case of dry rhyolite lava, with a limited porosity at atmospheric pressure, that implies a high temperature in the range 850–900 °C (Stevenson et al. 2001). The coherent rhyolite lava that avoided direct contact with water was also emplaced in the form of shallow intrusions – cryptodomes (section in the Fig. 2, Fig. 17E, Figs. S27–S29 in the El. Suppl. 2). Meanwhile, the surface of the "dome" was exposed to weathering and further disintegration of glassy material took place due to related epigenetic processes (Figs. S21–S22 in the El. Suppl. 2). The loose material was mobilized, reworked and laid down on alluvial fans at the base of the "dome" (Fig. 2, Figs. S23–S24 in the El. Suppl. 2). The alternation of massive matrix supported breccias with moderately sorted breccias and coarse sandstones points to reworking by debris and hyperconcentrated flows, initiated by torrential precipitation (cf. Cas & Wright 1988).

A few metres thick mantle of tuffs represents a product of the last event in the evolution of the volcano (Figs. 2 and 17E, Fig. S25 in the El. Suppl. 2). Mantle bedding and a high degree of sorting point to the fall type deposits with the exception of rare massive horizons of unsorted tuff at the feet of the "dome" that were laid down by pumice and ash flows. As mentioned above, fine to coarse grained tuffs are composed of disintegrated glassy material of the "dome". Thus, the relevant explosive activity combined aspects of the vulcanian and phreatic types of eruptions that associate with the growth of extrusive domes (cf. Heiken & Wohletz 1987).

The Jastrabá perlite deposit

In the Jastrabá perlite deposit we do not have any evidence of the presence of a groundwater-bearing aquifer or any signs of initial phreatomagmatic activity. Based on the succession and lithology of units (Fig. 3) we can reconstruct the evolution of the monogenetic rhyolite volcano hosting the deposit (Fig. 18). A north-south striking fault served as a conduit for ascending magma. The absence of a fall tuff horizon at the base of the volcano indicates that magma reached the surface in a degassed state and its extrusion to the surface was not accompanied by significant explosive activity. Viscous rhyolite magma later formed a growing extrusive dome that was apparently asymmetric due to an escarpment at the fault (east of the fault the ground was at lower elevation – Figs. 3 and 18). Growth of the extrusive dome is generally accompanied by processes that lead to the accumulation of glassy breccias. At the surface of extrusive domes, fast cooling of viscous lava creates a craggy carapace of glassy lava that owing to thermal contraction and further expansion of the domes disintegrates into a cover of glassy breccia (cf. Williams 1932; Fink & Anderson 2000; Wadge et al. 2009). Gravity driven avalanches move loose glassy brecciated material down the steep slopes of the domes where it accumulates as talus, forming a talus apron at the base of the domes (cf. Williams 1932; Francis 1993). At the same time, repeated collapses at the over-steepened sides of the domes give rise to block-and-ash flows (nuée ardentes) that show a higher mobility and transport material from sides of the domes further on gently sloping fans surrounding the domes (cf. Francis 1993; Freundt et al. 2000). So, the further growth of the asymmetric Jastrabá skala dome was accompanied by brecciation and by a significant accumulation of glassy talus breccia at its eastern side (future perlitic breccias of the deposit – Fig. 18B–D, Figs. S35–S36 in the El. Suppl. 2) and at the same time by the deposition of block-and-ash flows with associated surge and fall type tuffs further eastward (Fig. S37 in the El. Suppl. 2). The dominantly contraction-driven fragmentation is preserved in the form of fragments and blocks in the breccia that are angular, often polygonal and some of them show a radial jointing due to a fast chilling following the disintegration (Van Otterloo et al. 2015). According to natural observations and analogue experiments with Bingham plastic, the height of the growing extrusive dome is limited by the yield strength and the extrusion

rate of lava (Fink & Griffith 1998). When the growing dome reaches a critical height, it starts to spread laterally. That was also the case of the Jastrabá skala extrusive dome (Fig. 18D). In the advanced stage of evolution, it started to spread laterally eastward and northward creating short and thick dome-flows (coulées) that pushed aside and covered partially the accumulation of glassy breccia created during the preceding stage of dome growth (Figs. 3 and 18).

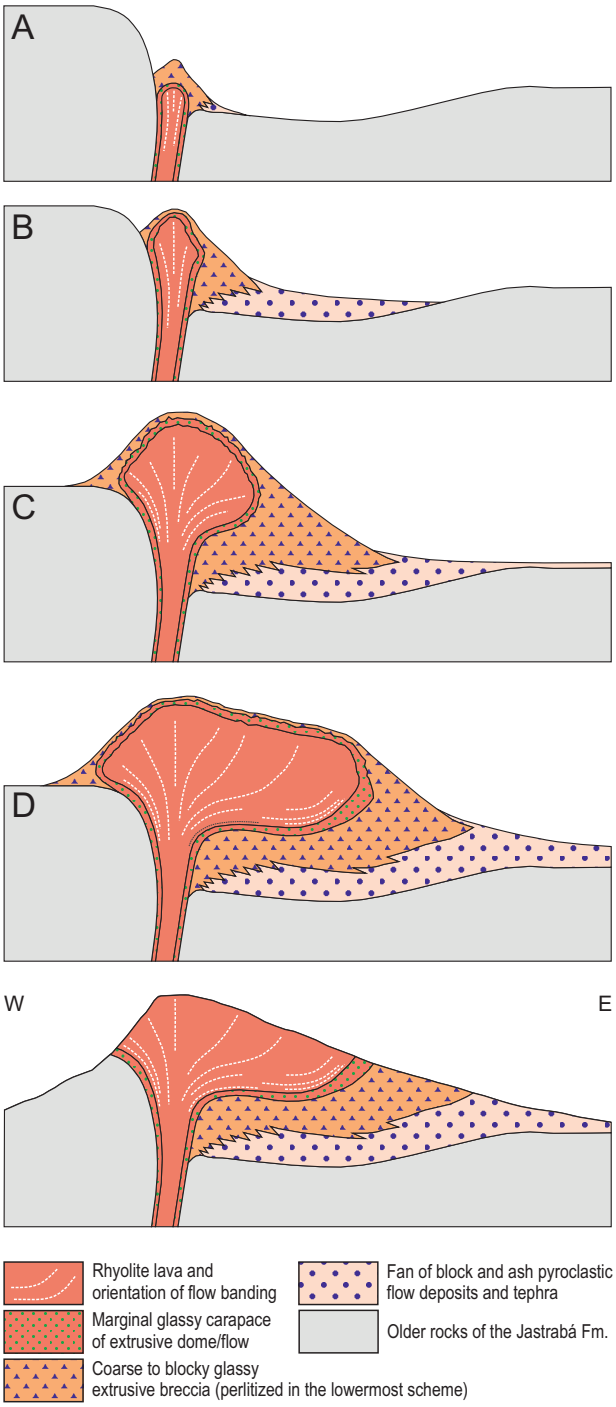

Fig. 18. A scheme of the Jastrabá perlite deposit and related volcano evolution. **A, B, C, D** — initial, early, advanced and final stages of the rhyolite lava extrusion and associated volcanoclastic apron deposition. The lowermost picture shows the present state following denudation.

Petrography of the Lehôtka pod Brehmi and Jastrabá perlite deposits

The perlites of both deposits are hydrated glassy rhyolites poor in phenocrysts. As far as phenocrysts are concerned, they are compatible with other types of the Jastrabá Fm. rhyolites (cf. Hojstričová 1982; Lexa et al. 1997; Demko et al. 2010). While the perlites of individual deposits show quite uniform petrographic composition, there are significant differences among the deposits. The LPB perlite is hydrated glassy rhyolite with phenocrysts of plagioclase and biotite and no K-feldspar or quartz phenocrysts. The volcanic products of both volcanic centres (early eastern and later western) show the same petrographic composition with the exception of the cryptodomes also containing minor amphibole phenocrysts. The JST deposit perlite is hydrated glassy quartz–sanidine–plagioclase rhyolite, with phenocrysts of plagioclase, biotite and minor quartz and sanidine, especially in associated pyroclastic flow deposits. In comparison with the LPB perlite, plagioclase phenocrysts are enriched in the Ab component (Table S1 and Fig. S1 in the El. Suppl. 4) and biotite phenocrysts are poorer in TiO_2 and MgO and enriched in FeO (Table S4 and Fig. S2 in the El. Suppl. 4), with the exception of a few biotite phenocrysts that show the same composition. These petrographic differences, as well as differences in chemical composition (see below) point to more evolved silicic magma in the case of the JST deposit perlite.

Microlites represent another interesting aspect of petrography. Microlites of pyroxenes and magnetite, including trichytes, have been observed only in the most degassed dark dense perlites. Only feldspar microlites occur in porous and pumiceous rhyolites, where the porosity implies an incomplete degassing. As the formation of glass corresponds to the quench fragmentation, microlites crystallized during the final stage of the magma ascent, most probably due to a combined effect of decompression driven degassing and related undercooling (cf. Blundy et al. 2006; Hammer 2008). The composition of feldspar microlites (Tables S2 and S3 in the El. Suppl. 4), Or rich plagioclase, Ab-rich sanidine and anorthoclase, implies a high temperature of crystallization (Fig. S1 in the El. Suppl. 4).

Most of the plagioclase phenocrysts show an intense fracturing (Figs. 8B and 9B). The pattern of fractures is the same as the pattern of fractures taking part in the quench fragmentation of glass. Apparently, the fracturing of plagioclase phenocrysts is related to the quench fragmentation of glassy rhyolite. A similar fracturing of plagioclase and quartz phenocrysts has been observed in phreatomagmatic pyroclasts of the silicic Puketarata tuff ring in New Zealand (Kosik et al. 2019).

Petrology of the Lehôtka pod Brehmi and Jastrabá perlite deposits

Perlites of the LPB and JST deposits, as well as rhyolites of the Jastrabá Fm., are subalkalic (Fig. 14), calc-alkalic

according to the criteria of Frost et al. (2001) (Fig. 15C), high-K according to the criteria of Peccerillo & Taylor (1976) (Lexa et al. 1997) and peraluminous with normative quartz and corundum (Demko in Demko et al. 2010). With andesites of the CSVF they form a bimodal association (Fig. 14), pointing to a separate origin of the rhyolite magma. While andesites are interpreted as a product of partial melting of a metasomatized lithospheric mantle (Harangi et al. 2007; Seghedi & Downes 2011) or partial melting of a lower crustal metabasic source associated with crustal contamination (Kohút et al. 2019), in the case of rhyolites the dominant role was played either by a partial melting of an amphibole-rich lower crustal plutonic source (Demko in Demko et al. 2010), or more probably by a segregation of rhyolitic melt from an amphibole-rich water saturated crystal mush in the upper crustal magma chamber (Rottier et al. 2020). P–T conditions in the magma chamber are estimated to have been 4.4–1. 5 kbar and 830–700 °C (Demko in Demko et al. 2010) and to ~2 kbar and 760–700 °C (Rottier et al. 2020).

Microlites crystallized during the final stage of the magma ascent. It follows that their thermometry provides an estimate of the eruption temperature. Algorithms of Putirka (2008), applied to plagioclase – alkali feldspar microlite pairs and feldspar microlite – liquid (glass) pairs, estimate the probable eruption temperature for the lava of the LPB deposit in the range 910–870 °C and for the lava of the JST deposit in the range 820–810 °C. The eruption temperature of the LPB rhyolite lava was roughly 100 °C higher than the crystal mush in the source magma chamber. Apparently, the eruption was initiated by a recharge of the magma chamber by a mafic magma of higher temperature. Such an event is recorded in the zonality of plagioclase phenocrysts with resorbed cores of relatively lower An content surrounded by an An enriched zone (Fig. 8B), by frequent resorption of phenocrysts and by the occurrence of rare mafic enclaves in the rhyolite/perlite. Viscosity and the glass transition temperature, calculated using the model of Giordano et al. (2008), were 8.8–8.3 Pas and 700 °C, respectively. These values are compatible with assumptions based on the occurrence of the relatively thin lava flow on the slope of the "dome" (see above). The eruption temperature of the JST deposit rhyolite lava was roughly the same as the temperature of the crystal mush in the source magma chamber. The eruption was in this case initiated by another mechanism, perhaps by exsolution of fluids from an oversaturated magma that lowered its apparent density and viscosity. The viscosity and the glass transition temperature, calculated using the model of Giordano et al. (2008), were 9.4–9.2 Pas and 665 °C, respectively. These values are compatible with the dome-flow form of extruded lava (cf. Fink & Griffith 1998).

The chemical composition of perlites (Table 2, El. Suppl. 6) confirms petrographic observations. Perlites of individual deposits show only a limited variability with no significant differences between lithological units or between dark dense and grey porous perlites of the LPB deposit, while there is a significant difference in the composition of perlites between the two deposits (Figs. 14 and 15, plots in the El. Suppl. 8). Perlites of the JST deposit are relatively enriched in silica and incompatible elements Ba, Nb, Th, U, light REE and relatively impoverished in all other analysed elements, including K, Rb and Zr that usually behave as incompatible elements during differentiation. Apparently, the JST deposit perlite in comparison with the LPB deposit perlite represents an extremely evolved silicic magma. However, the comparison with other rhyolites of the Jastrabá Fm. indicates that perlite composition in the two deposits is not unusual in the framework of the whole Jastrabá Fm. Plots of Na_2O+K_2O, Total Fe oxides, MgO, Al_2O_3, Ba, Sr vs. SiO_2 (Figs. 14 and 15D, El. Suppl. 8) demonstrate that the perlite compositions of the two deposits cannot be related via a simple differentiation trend. This supports the idea that rhyolite magmas were generated by a segregation of rhyolitic melt from an amphibole-rich water-saturated crystal mush in the upper-crustal magma chamber (Rottier et al. 2020) that was spatially inhomogeneous (cf. geochemical groups of the Jastrabá Fm. rhyolites of Demko in Demko et al. 2010).

Glass composition

The discussion on glass composition is based on analyses recalculated on the water-free basis (Table 3, El. Suppl. 7). Naturally, taking into account the phenocryst assemblages of perlites, the composition of pure glass, if compared to perlite, shows an important relative enrichment in silica, a slight enrichment in alkalis and a relative impoverishment in Al_2O_3, TiO_2, Total Fe oxides, MgO and CaO. On average, glass of the JST deposit perlite, if compared with glass of the LPB deposit perlite, is richer in silica and poorer in Al_2O_3, TiO_2, CaO and K_2O (Table 3). There is no real difference in the composition of perlite glass from the eastern and western parts of the LPB deposit. EPMA spot analyses of the glass show much higher dispersion than the compositions of corresponding samples of homogenized perlite (Figs. 14 and 15, El. Suppl. 8). This can be explained by the small size of analysed spots (10 μm), a lesser precision of EPMA analyses and a local variability in glass composition. However, in the case of alkalis, variability in their individual concentrations in glass is extremely high (Fig. 15A, B) and needs a different explanation. One of the possibilities would be the variability between samples. To test such an assumption, we have constructed a K_2O vs. SiO_2 plot for glass compositions of grey porous perlites of the LPB deposit, where points are distinguished according to individual samples (Fig. 15E). The plot demonstrates clearly that the contribution of variability between samples to the larger dispersion of K_2O contents in glass is relatively small. So, the large dispersion of alkalis is related mostly to the variability in their contents on a local scale of individual thin sections (El. Suppl. 7) or even on a local scale of tenths of millimetres as documented by the location of individual analyses in the thin sections. While the dispersion of Na_2O and K_2O individually is extremely high (Fig. 15A, B), dispersion of their sum is much smaller (Fig. 14), comparable with

dispersion of other oxides. It follows, that there exists a mutual exchange among Na_2O and K_2O, a kind of segregation into small domains enriched either in Na_2O or K_2O. Their K_2O/Na_2O ratio varies from 1.0 to 4.0 in the LPB deposit and in the range from 1.4 to 7.0 in the JST deposit. The same phenomenon has been described by Jezek & Noble (1978) on the basis of their EPMA study of obsidian-perlite pairs. Such a pre-crystallization grouping of cations in glass, corresponding to structural ordering and lowering of the system energy, was discussed extensively by Ashikhmina et al. (1987). The silica content of glass in perlites of the LPB deposit varies in the range 75.4–79.0 wt. % and in perlites of the JST deposit in the range 76.4–79.5 wt. %. Despite the large dispersion of glass projection points in plots, with exception of K_2O, all oxides show inexpressive negative trends with increasing silica content. This might be related to the closure effect of analytical data given in percentages, where a certain extent of negative correlation results from a decrease of other element values with an increase in the silica content (Chayes 1960).

The water content of perlites varies in the range 3.1–5.1 wt. % at the LPB deposit and in the range 3.4–6.0 wt. % at the JST deposit (Tables 2 and 4). The variability of the glass water content is much higher – 1.5–7.3 wt. % for the LPB deposit and 2.8–7.4 wt. % for the JST deposit (Table 3). While the average LOI of dark dense perlites at the LPB deposit is slightly lower than the average LOI of grey porous perlites (Table 4) there is no obvious difference in water contents of their glasses (Table 3, Fig. 16). Naturally, one would expect that the porosity enhances the process of secondary hydration. However, it appears that it does not play a dominant role in the final degree of hydration of the volcanic glass. Plots in the Fig. 16 and additional plots in the El. Suppl. 8 illustrate the relationship between perlites and perlite glass water contents to their chemical composition. Despite a high variability of water contents for any given silica concentration, the water contents show generally a tendency to increase with the increasing silica content (Fig. 16A). Such a relationship is expected if water during hydration reacts with the silicate network to form silanol groups (Van Otterloo et al. 2015) and the silanol groups contribute to the water sorption capacity of porous materials (Ng & Mintova 2008). Water does not show any relationship with the concentration of other oxides in glass except for Na_2O concentration that generally decreases with the increasing water content of glass. It follows that the amount of hydration water in our perlites is not controlled by the composition of their glass with the exception of increasing ability to absorb water with increasing silica content. The observed general decrease of Na_2O with the increasing water content (Fig. 16B) might be related to a possible hydrogen exchange with Na^+ ions during the process of hydration (Cerling et al. 1985).

Perlite porosity

The porosity is a very important aspect of perlite deposits as it affects fragmentation of perlites, their secondary hydration, crushing and expansion. Low porosity enhances quench fragmentation while high porosity has an opposite effect due to arresting of propagating fractures (Van Otterloo et al. 2015). The porosity, especially when it involves open interconnected pores, helps the process of secondary hydration by sorption of water in micro- and nano-pores (Bagdassarov et al. 1999; Ng & Mintova 2008; Kaufhold et al. 2014) and allowing a fast transport of water or steam through porous glass.

As mentioned above, rhyolite magma was probably extracted from a crystal mush at the pressure of around 2 kbar and temperature of 800–700 °C. In these conditions, a silicic magma contains roughly 3–5 wt. % water (Holtz et al. 2001). As the rhyolite magma in our study has reached the surface almost dry, water was lost during the ascent by continuous degassing due to decompression (Eichelberger 1995). The decompression leads at first to water saturation and subsequently to exsolution of vapour in the form of bubbles. In a viscous rhyolite melt bubbles are not able to migrate. So, to make degassing effective permeable foam must have been formed – such a situation is established when the vesicularity reaches 60–70 % (Eichelberger 1995). However, shear deformation that causes elongation and coalescence of the bubbles, results in an increase in the lava permeability and thus an efficient degassing can occur at much lower vesicularity (Okumura et al. 2009; Shields et al. 2016). The final stage of degassing is associated with compaction and retrograde welding – sheared elongated pores collapse to narrow planes or disappear entirely. It follows that the relatively older narrow stretched pores observed in both types of our perlites (Fig. 10C, E, F), dark dense as well as grey porous, represent remnants of pores that enabled outgassing of magma during its ascent (Shields et al. 2016). This is confirmed by the preservation of interconnected pores, even in dark dense perlites with low porosity and the prevalence of narrow stretched pores (Fig. 11, Varga et al. 2019). Despite the process of continued degassing, the magma reaches the low-pressure surface environment with the water content of a few tenths of percent. This is enough to create the observed open pores with vesicularities reaching 45 % (Fig. 11, Eichelberger 1995). It was preserved because of melt freezing during the quench fragmentation. Open pores are often undeformed (Fig. 10A, C). That points to their growth immediately before quenching.

Genesis of perlites at the Lehôtka pod Brehmi and Jastrabá deposits

Petrological processes leading to the volcanic activity of phenocryst-poor rhyolites and volcanic processes leading to large enough accumulations of glassy rhyolite breccia have already been discussed above. Here we shall discuss aspects of their secondary hydration.

Water occurs in hydrated glass in the molecular form (H_2O) and in hydroxyl groups (OH) (Stolper 1982). Hydroxyl groups are bound in the structure of glass (Zotov et al. 1992) and mostly represent remnants of magmatic water left after degassing prior to and during an eruption (Friedman & Smith 1958; Eichelberger 1995). Its concentration in glass is usually just

a few tenths of one percent and it is controlled dominantly by the pressure at which the glass transition has taken place (DeGrout-Nelson et al. 2001). Molecular water is absorbed in pores/fractures, micro-pores/micro-fractures and nano-pores/nano-fractures, where it is bound by capillary forces and silanol groups attraction (Bagdassarov et al. 1999; Ng & Mintova 2008; Kaufhold et al. 2014) and introduced into glass by diffusion (Zhang & Behrens 2000), where it occupies domains of disorder (Zotov et al. 1992). It is generally interpreted as secondary water as there is almost no molecular water present in fresh obsidian at the time of its origin (Zhang et al. 2007).

On the basis of the H/D isotopic ratio of perlites Friedman & Smith (1958) concluded that the hydration water in perlites is of meteoric origin and the secondary hydration took place in the ambient conditions. The uptake of meteoric water following the deposition of volcanic glass in the form of pumice and/or ash has been widely used in palaeoclimatic studies (e.g., Friedman et al. 1993; Canavan et al. 2014). However, at low temperature, the water diffusion in volcanic glass is very slow (Friedman & Long 1976; Zhang & Behrens 2000). Intense fracturing and/or porosity were incorporated into secondary hydration models to explain the pervasive perlitization of larger volumes of glass (Denton at al. 2012; Giachetti & Gonermann 2013; Van Otterloo et al. 2015). Alternatively, there are several works that advocate a faster hydration at increased temperature to avoid the problem of the low diffusion rate (Kano et al. 2010; Von Aulock et al. 2013; Bindeman & Lowenstern 2016; Martin et al. 2017; Hudak & Bindeman 2018).

Koděra et al. (2019) investigated stable isotopes (H/D and $^{16}O/^{18}O$) in perlites of the LPB and JST deposits and other localities. A careful interpretation of stable isotope data, including modelling of fractionation and mixing with present day meteoric water, enabled them to conclude that the hydration of glass most probably occurred by a mixture of heated meteoric liquid and vapour. Particularly important is the significant participation of hot vapour that could enable an easy penetration into porous rock compared to liquid water. Furthermore, vapour has an order of magnitude lower viscosity compared to aqueous liquid and has no surface stress. The hydration started at elevated temperatures, but a higher degree of hydration happened by removal of alkali elements accompanied by exchange for diffusing ions of hydrogen at significantly lower temperatures (Cerling et al. 1985). This is also supported by the fact that the diffusivity of molecular water in glass increases exponentially with the total water concentration in the glass (Zhang & Behrens 2000). The interpreted mean final hydration temperatures (final isotopic equilibrium) were ~55 °C for LPB deposit perlites and ~37 °C for JST deposit perlites, so the intensity of hydration is likely proportional to the final temperature of hydration (i.e., opening of the system for an efficient diffusion of water into glass).

Despite the knowledge that vapour can efficiently enter even tiny pores, the advanced hydration could occur just in a sufficiently porous glass to overcome the problem of the low diffusion rate (Koděra et al. 2019). The porosity of perlite from both deposits was studied extensively by Varga et al. (2019). 3D tomography demonstrated that perlites have enough open connected pores (Fig. 11) to effectively channel water and/or steam to enable pervasive hydration in a relatively short time. A thermal treatment of perlite samples (Varga et al. 2019) confirmed that most of the hydration molecular water is bound to pores/fractures, micro-pores/micro-fractures and nano-pores/nano-fractures, as already advocated by Bagdassarov et al. (1999) and Kaufhold et al. (2014). However, FTIR spectrometry of thermally treated samples has documented that at higher temperatures a loss of OH groups has also occurred, which implies a further loss of water dissolved in the glass among pores and fractures via diffusion (Varga et al. 2019).

Dark dense perlites of the LPB deposit show total porosity of 15.7–0.9 % and interconnected porosity of 13.0–0.3 % (Fig. 11, Varga 2018). Compared to grey porous perlites they show slightly lower water content (Table 4). Apparently, the interconnected porosity is high enough to facilitate a pervasive hydration at elevated temperatures. However, owing to a larger distance between pores, the pervasive hydration at lower temperature is limited due to the significantly lower diffusion rate (Zhang & Behrens 2000) which impedes progressive hydration with decreasing temperature.

As shown by Koděra et al. (2019), a higher degree of hydration happens at progressively decreasing temperatures. This probably occurs in geological settings that enable slow cooling so that the decreasing speed of diffusion with decreasing temperature (Zhang & Behrens 2000) is compensated by a longer time of opening of the system, namely a prolonged stay at an increased temperature is required in the contact with heated meteoric water, especially in the form of vapour. Considering the form of the Jastrabá skala extrusive dome-flow, the duration of its growth can be estimated at 100–300 days using the approach of Fink & Griffith (1998) and Lyman et al. (2004). During this time and the subsequent time of cooling that lasts for months to years (Von Aulock et al. 2013; Bindeman & Lowenstern 2016) the accumulation of glassy breccia was kept at an elevated temperature. Apparently, in combination with the high porosity, it was sufficient for a complete hydration to take place. In the case of the LPB deposit we can expect even a longer time because of the insulation by the cover of tuffs and a longer-lasting flow of steam from deeper parts of the volcanic conduit, where the still hot lava remained in the contact with groundwater.

Properties of perlites and applications

Expanded perlite is the main commercial product of perlite mining. The quality of expanded perlite depends on the technology (processing line, temperature, particle size etc.) and natural perlite properties (the content of water and its strength of bonds, density, porosity, chemical composition, the amount and size of mineral admixtures and texture of rock; Naert et al. 1980; Zähringer et al. 2001; Barker & Santini 2006; Roulia et

al. 2006; Tsikouras et al. 2016). A specific influence of perlites properties from the CSVF on the quality of expanded perlite will be highlighted in the following part.

The mineral admixture in perlites is relatively low, averaging less than 6–7 wt. % in both mined perlite deposits (Table 1). Such a low amount does not have a significant effect on the expansion of perlite. Sedimentation tests of perlites after expansion in Imphoff cones showed that only half of the mineral admixtures were hosted by the unexpanded fraction. The rest of the mineral admixtures remained in the expanded perlite (Varga 2018). A significant negative influence of higher mineral admixture upon the quality of the expanded perlite has been demonstrated in the case of the Malá Bara perlite deposit in Eastern Slovakia. Over 30 wt. % of phenocrysts increase here the bulk density of the expanded perlite so much that the deposit is not suitable for exploitation (Zuberec et al. 2005; Varga 2018).

The most important factor for the expansion of perlite is the presence of 2–5 wt. % of water. Its effort to expand at the low pressure and temperature 800–1100 °C causes transformation of perlite into a glass foam and reduction of the raw perlite bulk density by 90 % (Breese & Barker 1994; Koukouzas et al. 2000; Barker & Santini, 2006; Tsikouras et al. 2016). Perlites from the CSVF contain 3–5 wt. % of water (Tables 2 and 4), predominantly in the form of molecular water (Varga et al. 2019; Pálková et al. 2020), as in the case of other world perlite deposits (Roulia et al. 2006). The degree of expansion and the bulk density, however, are not the same. The degree of expansion of perlite from other world deposits is significantly higher. Greek perlite expands even 2.5-times more than perlites from the CSVF (Varga 2018). The main reasons for variable expansion are different strength of water bond and the chemistry of perlites (Varga et al. 2019). They studied the release of water in respect to temperature, time, grain size, porosity and water content. Perlites from the LPB and JST deposits show approximately the same amount of loosely bound water released in the temperature range of 0–250 °C as of moderately bound water released in the range of 250–550 °C. This seems to be the first factor that causes a lower degree of expansion of Slovak perlites in comparison with perlites from other world deposits that release more water in the range 250–550 °C. The second factor is a lower ratio of Na to K. Perlites from CSVF have higher K_2O content (5.16–5.62 wt. % on average, Tables 2 and 3, Fig. 15A, B) in comparison with perlites elsewhere (2.68–4.82 wt. %, Roulia et al. 2006; Varga et al. 2019). On the other hand, the content of Na_2O is significantly lower in perlites of CSVF (2.08–2.68 wt. % on average, Tables 2 and 3, Fig. 15A, B) in comparison with perlites elsewhere (2.95–4.26 wt. %, Roulia et al. 2006; Varga et al. 2019). Perlites of CSVF show ratios of K_2O/Na_2O between 2.0 and 2.6, while perlites elsewhere between 1.0 and 1.4 and some Greek perlites even only 0.6. The higher amount of sodium decreases the perlite's viscosity during the thermal expansion and the lower viscosity increases the degree of expansion and final radius of expanded perlite grains (Hess et al. 1995; Zähringer et al. 2001). The lower viscosity also causes thinning of bubble walls and in that way a lesser mechanical strength of expanded perlite grains (Zähringer et al. 2001; Varga et al. 2019). It follows that CSVF perlites show a lower degree of expansion, have thicker bubble walls and show a higher mechanical stability in comparison with perlites elsewhere (Varga 2018).

Perlite porosity is another phenomenon that can influence the process of perlite expansion, although not so significantly as water and alkali contents. Varga et al. (2019) have demonstrated that the initial raw perlite porosity, the pore size and shape can affect the final porosity after milling. After milling, the porosity of perlite with homogenous distribution of large pores decreases while the porosity of perlite with heterogeneous distribution of pores, with their variable size and forms, increases. Although a direct relation between the porosity and the water release from perlite was not confirmed, the general relationship between the bulk density and the expansion of Slovak perlites has been documented (Hroncová et al. 1991; Varga 2018) and the porous fine-grained perlite (0.16–0.3 mm) from the LPB deposit showed a higher degree of expansion than the dense perlite from this deposit (Varga 2018; Varga et al. 2019). Measurement of the bulk density (the property significantly affected by porosity) of the raw perlite is clearly one of the important aspects when assessing perlite quality. The importance of the bulk density from the point of view of perlite quality is even higher in the case of a heterogenous deposit such as that at Lehôtka pod Brehmi (Blišťan et al. 2020).

Conclusions

The paper brings an up-to-date interpretation of the geology, properties and genesis of two perlite deposits from the Central Slovakia Volcanic Field after several years of field work, microscopic study and laboratory investigations. After a long time, it is the first systematic characterization of exploited perlite deposits.

The Lehôtka pod Brehmi (LPB) perlite deposit is hosted by remnants of a monogenetic rhyolite volcano the evolution of which was governed by a groundwater/magma interaction. The productive perlite zone is represented by extruded hyaloclastite breccias composed of grey porous and dark dense fragments. The Jastrabá (JST) perlite deposit is represented by an accumulation of glassy rhyolite breccia (grey porous blocks and fragments) associated with the evolution of an extrusive dome/coulée.

Perlites at both deposits are poor in phenocrysts. Their average glass content is 94.5 wt. % (LPB) and 95.8 wt. % (JST). Phenocryst assemblages include plagioclase, biotite and minor amphibole in perlite of the LPB deposit and plagioclase, biotite and minor sanidine/anorthoclase in perlite of the JST deposit. Feldspar microlites in glass of both deposits are of plagioclase, anorthoclase and sanidine composition. Glass at both deposits is silica rich (LPB ~76.6 %, JST ~78.1 %) with other major constituents represented by Al_2O_3 (LPB ~12.7 %,

JST ~12.4 %), Na_2O (LPB ~2.6 %, JST ~2.5 %) and K_2O (LPB ~5.6 %, JST ~5.1 %) (data in wt. % dry). Glass at both deposits is inhomogeneous on the microscopic scale showing domains enriched in Na_2O or K_2O, respectively. Perlite water content varies in the range 3.1–5.1 wt. % (LPB) and 3.4–6.0 wt. % (JST). Glass water content shows a weak positive correlation with its silica content, reflecting a dominant role of silanol groups in water bounding and a negative correlation with its Na_2O content, reflecting removal via the exchange for diffusing ions of hydrogen.

Perlites of the LPB and JST deposits are peraluminous, calc-alkalic and of the high-K type. Their parental rhyolite magma apparently originated by the segregation of a rhyolitic melt from an amphibole-rich water-saturated crystal mush in the upper crustal magma chamber (P=3.3–1.4 kbar). The magma temperature in the chamber was most probably in the case of the LPB deposit in range 820–700 °C and in the case of the JST deposit in the range 825–800 °C. Based on the feldspar microlites thermometry, the probable eruption temperature for the LPB perlite was in the range 910–870 °C and for the JST perlite in the range 820–810 °C. Eruption lava viscosities and glass transition temperatures were calculated to 8.8–8.3 Pas and 700 °C for the LPB perlite and 9.4–9.2 Pas and 665 °C for the JST perlite. These values are compatible with presented evolution models for both volcanoes hosting the perlite deposits.

With a few exceptions among the dark dense ones, perlites show porosities in the range 12–44 %, with most of the pores being interconnected. There are two types of pores present: narrow stretched ones that represent remnants of pores that enabled outgassing of magma during its ascent and open undeformed ones that grew at a low pressure immediately before quenching.

The transformation of volcanic glass into perlite took place owing to hydration by heated fluids of the meteoric origin. The hydration was supported by a significant porosity with interconnected pores and by sustainable elevated temperature lasting months to several years in favourable geological conditions.

The perlites of the Central Slovakia Volcanic Field show a lower degree of expansion compared to perlites from some other world deposits. Perlites at both studied deposits show a lower content of tightly-bound water and a lower ratio of Na to K. These properties are responsible for their lower degree of expansion. On the other hand, due to the same reason the Central Slovakia Volcanic Field perlites have better mechanical stability.

Acknowledgements: The authors gratefully acknowledge financial support from the Slovak Research and Development Agency (project no. APVV-0339-12) and the Slovak Grant Agency (VEGA, projects no. 2/0162/11, 2/0138/15, 1/0196/19). LBK PERLIT, Ltd. is acknowledged for permission to do fieldwork with sampling in both their perlite deposits. N. Halašiová and Ľ. Puškelová are acknowledged for carrying out the SEM images and XRD analysis of oriented samples, respectively. We are grateful to reviewers Károly Németh and János Szepesi for suggestions that improved the manuscript.

References

Ashikhmina N.A., Bogatikov O.A., Dikov Yu.P., Frikh-Khar D.I., Cimbálniková, A., Zemčík T., Klečka M., Kos M., Mikeš J., Palivcová M. & Cílek V. 1987: Natural glasses – indicators of geological processes. *Nauka,* Moscow, 1–157 (in Russian).

Austin-Erickson A., Büttner R., Dellino P., Ort M.H. & Zimanowski B. 2008: Phreatomagmatic explosions of rhyolitic magma: Experimental and field evidence. *Journal of Geophysical Research* 113, B11201. https://doi.org/10.1029/2008JB005731

Bagdassarov N., Ritter F. & Yanev Y. 1999: Kinetics of perlite glass degassing: TG and DSC analysis. *Glass Science Technology* 72, 277–290.

Barker J.M. & Santini K. 2006: Perlite. In: Kogel E.J. (Ed.): Industrial minerals and rocks. *Society for Mining, Metallurgy, and Exploration, Inc*., Littleton, Colorado, 685–702.

Beňo J. & Očenáš D. 1962: Lehôtka pod Brehmi – perlite, final report and reserves assessment. *Open file report, Archive of the State Geological Institute of D. Štúr*, Bratislava, 1–79 (in Slovak).

Bindeman I.N. & Lowenstern J.B. 2016: Low-δD hydration rinds in Yellowstone perlites record rapid syneruptive hydration during glacial and interglacial conditions. *Contributions to Mineralogy and Petrology* 171, 89. https://doi.org/10.1007/s00410-016-1293-1

Blišťan P., Jacko S., Kovanič Ľ., Kondela J., Pukanská K. & Bartoš K. 2020: TLS and SfM approach for bulk density determination of excavated heterogeneous raw materials. *Minerals* 10, 174.

Blundy J., Cashman K. & Humphreys M. 2006: Magma heating by decompression-driven crystallization beneath andesite volcanoes. *Nature* 443, 76–80. https://doi.org/10.1038/nature05100

Bouška V., Borovec Z., Cimbálniková A., Kraus I., Lajčáková A. & Pačesová M. 1993: Natural glasses. *Academia,* Praha, 1–339.

Breese R.O.Y. & Barker J.M. 1994: Perlite. In: Carr D.D. (Ed.): Industrial Minerals and Rocks, 6th edition. *Society for Mining, Metallurgy, and Exploration, Inc*., Littleton, Colorado, 735–749.

Canavan R.R., Carrapa B., Clementz M.T., Quade J., DeCelles P.G. & Schenbohm L.M. 2014: Early Cenozoic uplift of the Puna Plateau, Central Andes, based on stable isotope paleoaltimetry of hydrated volcanic glass. *Geology* 42, 447–450. https://doi.org/10.1130/G35239.1

Cas R.A.F. & Wright J.V. 1987: Volcanic successions, ancient and modern. *Chapman & Hall*, London, 1–528.

Cerling T.E., Brown F.H. & Bowman J.R. 1985: Low-temperature alteration of volcanic glass: Hydration, Na, K, ^{18}O and Ar mobility. *Chemical Geology (Isotope Geoscience Section)* 52, 281–293.

Chayes F. 1960: On correlation between variables with a constant sum. *Journal of Geophysical Research* 65, 4185–4193.

Chernyshev I.V., Konečný V., Lexa J., Kovalenker V.A., Jeleň S., Lebedev V.A. & Goltsman Y. V. 2013: K–Ar and Rb–Sr geochronology and evolution of the Štiavnica Stratovolcano (Central Slovakia). *Geologica Carpathica* 64, 327–351.

DeGroat-Nelson P.J., Cameron B.I., Fink J.H. & Holloway J.R. 2001: Hydrogen isotope analysis of rehydrated silicic lavas: implications for eruption mechanisms. *Earth and Planetary Science Letters* 185, 331–341.

Demko R. Lexa J., Koděra P., Biroň A., Smolka J., Šesták P., Konečný P., Tuček Ľ., Ferenc Š., Bačo P., Repčiak M., Kollárová V., Kyška-Pipík R., Mikušová J., Kotulová J., Bystrická G. & Vlachovič J. 2010: Maps of paleovolcanic reconstruction of Slovak rhyolite volcanics and analysis of magmatic and hydrothermal processes. *Open file report*, *Archive ŠGÚDŠ*, Bratislava, 1–728 (in Slovak).

Denton J.S. Tuffen H. & Gilbert J.S. 2012: Variations in hydration within perlitised rhyolitic lavas – evidence from Torfajökull, Iceland. *Journal of Volcanology and Geothermal Research* 223–224, 64–73.

Eichelberger J.C. 1995: Silicic volcanism: Ascent of viscous magmas from crustal reservoirs. *Annual Review of Earth and Planetary Sciences* 23, 41–63.

Fink J.H. & Anderson S.W. 2000: Lava domes and coulees. In: Sigurdsson H., Houghton B.F., McNutt S.R., Rymer H. & Stix J. (Eds.): Encyclopedia of Volcanoes. *Academic Press*, San Diego, 307–319.

Fink J.H. & Griffith R.W. 1998: Morphology, eruption rates, and rheology of lava domes: Insights from laboratory models. *Journal of Geophysical Research* 103, 527–545.

Fink J.H., Malin M.C. & Anderson S.W. 1990: Intrusive and extrusive growth of the Mount St Helens lava dome. *Nature* 348, 435–437.

Forgáč J., Brestenská E., Klabenová K., Planderová E., Sitár V. & Škvarka L. 1974: Structural boreholes HF-1 (Hliník nad Hronom) and JL-1 (Jalná). *Regionálna geológia Západných Karpát* 4, 1–109 (in Slovak).

Francis P. 1993: Volcanoes, a planetary perspective. *Oxford University Press*, Oxford, 1–443.

Freundt A, Wilson C.J.N. & Carey S.N. 2000: Ignimbrites and block-and ash flow deposits. In: Sigurdsson H., Houghton B.F., McNutt S.R., Rymer H. & Stix J. (Eds.): Encyclopedia of volcanoes. *Academic Press*, San Diego, 581–599.

Friedman I. & Long W. 1976: Hydration rate of obsidian. *Science* 91, 347–352.

Friedman I. & Smith R.L. 1958: The deuterium content of water in some volcanic glasses. *Geochimica et Cosmochimica Acta* 15, 218–228.

Friedman I., Gleason J. & Warden A. 1993: Ancient climate from deuterium content of water in volcanic glass. *Geophysical Monograph* 78, 309–319.

Frost B.R., Barnes C.G., Collins W.J., Arculus R.J., Ellis D.J. & Frost C.D. 2001: A geochemical classification for granitic rocks. *Journal of Petrology* 42, 2033–2043. https://doi.org/10.1093/petrology/42.11.2033

Giachetti T. & Gonermann H.M. 2013: Water in volcanic pyroclast: Rehydration or incomplete degassing? *Earth and Planetary Science Letters* 369–370, 317–332. https://doi.org/10.1016/j.epsl.2013.03.041

Giordano D., Russell G. & Dingwell D.B. 2008: Viscosity of magmatic liquids: A model. *Earth and Planetary Science Letters* 271, 123–134. https://doi.org/10.1016/j.epsl.2008.03.038

Hammer J.E. 2008: Experimental Studies of the Kinetics and energetics of Magma Crystallization. In: Putirka K.D. & Tepley F.J. (Eds.): Minerals, Inclusions and Volcanic Processes. *Reviews in Mineralogy and Geochemistry* 69, 9–60. https://doi.org/10.2138/rmg.2008.69.2

Harangi Sz., Downes H., Thirlwall M. & Gméling K. 2007: Geochemistry, petrogenesis and geodynamic relationships of Miocene calc-alkaline volcanic rocks in the Western Carpathian arc, eastern central Europe. *Journal of Petrology* 48, 2261–2287. https://doi.org/10.1093/petrology/egm059

Heiken G. & Wohletz K. 1987: Tephra deposits associated with silicic domes and lava flows. *Geological Society of America Special Paper* 212, 55–76.

Hojstričová V. 1982: Mineralogical–petrographic characteristics of the Central Slovakia rhyolites. *Theses, Archive of the State Geological Institute of D. Štúr*, Bratislava, 1–120 (in Slovak).

Holtz F., Johannes W., Tamic N. & Behrens H. 2001: Maximum and minimum water contents of granitic melts generated in the crust: a reevaluation and implications. *Lithos* 56, 1–14. https://doi.org/10.1016/S0024-4937(00)00056-6

Hroncová Z. 1989: Perlite in the Central Slovakian neovolcanic area. *Mineralia slovaca* 21, 561–564 (in Slovak).

Hroncová Z. 1994: Jastrabá perlite deposit – reserves assessment. *Open file report, Archive of the State Geological Institute of D. Štúr*, Bratislava, 1–7 (in Slovak).

Hroncová Z., Sýkora J. & Viest Ľ. 1991: Jastrabá perlite deposit – final report on detail exploration. *Open file report, Archive of the State Geological Institute of D. Štúr*, Bratislava, 1–77 (in Slovak).

Hudak M.R. & Bindeman I.N. 2018: Conditions of pinnacle formation and glass hydration in cooling ignimbrite sheets from H and O isotope systematics at Crater Lake and the Valley of Ten Thousand Smokes. *Earth and Planetary Science Letters* 500, 56–66. https://doi.org/10.1016/j.epsl.2018.07.032

Jezek P.A. & Noble D.C. 1978: Natural hydration and ion exchange of obsidian: An electron microprobe study. *American Mineralogist* 63, 266–273.

Kano K., Yoshimura Y., Ishiyama D., Matsubaya O. & Ohguchi T. 2010: High-temperature hydration and explosive fragmentation of glassy rhyolite at Katsuma-Yama volcano, Okushiri Island, Hokkaido, Japan. *Int. Conf. Cities on Volcanoes, Tenerife, Abstract volume*, 7.

Kaufhold S., Reese A., Schwiebacher W., Dohrmann R., Grathoff G.H., Warr L.N., Halisch M., Müller C., Schwartz-Schampera U. & Ufer K. 2014: Porosity and Distribution of water in Perlite from the Island of Milos, Greece, *SpringerPlus* 3, 598. https://doi.org/10.1186/2193-1801-3-598

Koděra P., Varga P., Uhlík P., Milovský R., Lexa J., Kohút M. & Fallick A.E. 2019: Hydration of volcanic glass and genesis of perlite deposits based on oxygen and hydrogen isotope data. In: *Proceedings of the 15th SGA Biennial Meeting, 27–30 August 2019*, Glasgow, UK, 2, 923–926.

Kohút M., Anczkiewicz R., Erban V., Kochergina Y.V., Magna T., Recio C., Yi K. & Broska I. 2019: The Miocene granitic rocks of the Central Slovakian Neovolcanic Field: Isotopic constraints. In: Hrdličková K. & Daňková L. (Eds.): *Abstract volume of the 17th Meeting of the Central European Tectonic Groups, CETEG 2019*, Rozdrojovice, 39.

Konečný V., Lexa J. & Planderová E. 1983: Stratigraphy of the Central Slovakia Neogene Volcanic Field. *Západné Karpaty: Séria Geológia* 9, 1–203 (in Slovak with English summary).

Konečný V., Lexa J. & Hojstričová V. 1995: The Central Slovakia Neogene volcanic field: a review. In: Downes H. and Vaselli O. (Eds.): Neogene and related magmatism in the Carpatho–Pannonian region. *Acta Volcanologica* 7, 63–78.

Konečný V., Lexa J., Halouzka R., Hók J., Vozár J., Dublan L., Nagy A., Šimon L., Havrila M., Ivanička J., Hojstričová V., Mihaliková A., Vozárová A., Konečný P., Kováčiková M., Filo M., Marcin D., Klukanová A., Liščák P. & Žáková E. 1998: Explanatory notes to the geological map of Štiavnické vrchy and Pohronský Inovec mountain ranges (Štiavnica Stratovolcano). *Geologická služba Slovenskej republiky*, Bratislava, 1–473 (in Slovak with English summary).

Konečný V., Lexa J. & Šimon L. 2003: Geologic structure and evolution of intravolcanic depressions in the area of Neogene volcanism in Central Slovakia. *Mineralia Slovaca* 35, 255–290.

Kosik S., Németh K., Lexa J. & Procter J.N. 2019: Understanding the evolution of a small-volume silicic fissure eruption: Puketerata Volcanic complex, Taupo Volcanic Zone, New Zealand. *Journal of Volcanology and Geothermal Research*, 383, 28–46. https://doi.org/10.1016/j.jvolgeores.2017.12.008

Koukouzas N.K., Dunham A.C. & Scott P.W. 2000: Suitability of Greek perlite for industrial applications. *Applied Earth Science: Transactions of the Institutions of Mining and Metallurgy: Section B* 109, 105–111. https://doi.org/10.1179/aes.2000.109.2.105

Kraus I., Šamajová E., Gerthofferová H. & Lajčáková A. 1980: Mineral composition and genesis of clays, zeolites and perlites. *Final report, Geologický ústav PriF UK*, Bratislava, 1–248 (in Slovak).

Kraus I., Šamajová E., Šucha V., Lexa J. & Hroncová Z. 1994: Diagenetic and hydrothermal alterations of volcanic rocks into clay minerals and zeolites (Kremnické Vrchy Mts., Western Carpathians). *Geologica Carpathica* 45, 151–158.

Kúšik D., Šoltés S. & Mižák J. 2019: Slovak minerals yearbook 2018. *State Geological Institute of D. Štúr*, Bratislava, 1–143.

Lange J.M. & Heide K. 1996: Pichstone, rhyolite and kaolin near Meißen, Saxony. *Chemie der Erde* 56, 511–521.

Le Bas M.J., Le Maitre R.W., Streckeisen A. & Zanettin B. 1986: A chemical classification of volcanic rocks based on the total alkali-silica diagram. *Journal of Petrology* 27, 745–750.

Lexa J. 1971: Forms of rhyolite bodies in surroundings of Žiar nad Hronom. *Geologické Práce – Správy* 56, 67–80 (in Slovak with English summary).

Lexa J. & Konečný V. 1998: Geodynamic aspects of the Neogene to Quaternary volcanism. In: Rakús M. (Ed.): Geodynamic development of the Western Carpathians. *Geologická služba Slovenskej republiky*, Bratislava, 219–240.

Lexa J. & Pécskay Z. 2010: Radiometric dating of rhyolites by conventional K–Ar method: methodical aspects. In: Kohút M. (Ed.): Dating of minerals and rocks, metamorphic, magmatic and metallogenetic processes, as well as tectonic events. *Štátny geologický ústav D. Štúra,* Bratislava, 21–22.

Lexa J. & Pošteková K. 2012: Eruptive styles of rhyolite volcanoes in the sedimentary basin setting: the case of the Jastrabá Fm. in Central Slovakia. In: Arentsen K., Németh K. & Smid K. (Eds): Fourth International Maar Conference, Auckland, New Zealand, Abstract volume. *Geoscience Society of New Zealand Miscellaneous Publication* 131A, 124–125.

Lexa J., Konečný P., Hojstričová V., Konečný V. & Köhlerová M. 1997: Petrological model of the Štiavnica stratovolcano. *Open file report, Archive of the State Geological Institute of D. Štúr*, Bratislava, 1–50 (in Slovak).

Lexa J., Halouzka R., Havrila M., Hanzel V., Kubeš P., Liščák P. & Hojstričová V. 1998: Explanatory notes to the geological map of the Kremnické vrchy mountain range. *Geologická služba Slovenskej republiky*, 1–308 (in Slovak with English summary).

Lexa J., Seghedi I., Nemeth K., Szakacs A., Konecny V., Pecskay Z., Fülöp A. & Kovacs M. 2010. Neogene–Quaternary Volcanic forms in the Carpathian–Pannonian Region: a review. *Central European Journal of Geosciences* 2, 207–275.

Lexa J., Rottier B., Yi K., Audétat A., Broska I., Koděra P. & Kohút M. 2019: Magmatic evolution of the Štiavnica volcano. *Proceedings of the Geologica Carpathica 70*, *Earth Science Institute SAS*, Bratislava, 83–86.

Lyman A.W., Koenig E. & Fink J.H. 2004: Predicting yield strengths and effusion rates of lava domes from morphology and underlying topography. *Journal of Volcanology and Geothermal Research* 129, 125–138. https://doi.org/10.1016/S0377-0273(03)00236-1

Martin E., Bindeman I., Balan E., Palandri J., Seligman A. & Villemant B. 2017: Hydrogen isotope determination by TC/EA technique in application to volcanic glass as a window into secondary hydration. *Journal of Volcanology and Geothermal Research* 48, 49–61. https://doi.org/10.1016/j.jvolgeores.2017.10.013

McPhie J., Doyle M. & Allen R.L. 1993: Volcanic textures: a guide to the interpretation of textures in volcanic rocks. *Centre for Ore Deposit and Exploration Studies, University of Tasmania*, Hobbart, 1–196.

Naert K.A., Wright L.A. & Thornton C.P. 1980: Geology of the perlite deposits of the No Agua Peaks, Taos County, New Mexico. *Open file Report, New Mexico Bureau of Mines and Mineral Resources* 162, 1–88.

Nasedkin V.V. 1996: The perlite–obsidian association as non-equilibrium natural system: conditions of occurrence, petrological significance. *Chemie der Erde* 56, 364–372.

Németh K., Pécskay Z., Martin U., Gméling K. Molnár F. & Cronin S.H. 2008: Hyaloclastites, peperites and soft-sediment deformation textures of a shallow subaqueous Miocene rhyolitic dome-cryptodome complex, Pálháza, Hungary. In: Thomson K. & Petford N. (Eds.): Structure and emplacement of high-level magmatic systems. *Geological Society, London, Special Publications* 302, 61–83.

Ng E.P. & Mintova S. 2008: Nanoporous materials with enhanced hydrophilicity and high water sorption capacity. *Microporous and Mesoporous Materials* 114, 1–26.

Okumura S., Nakamura M., Takeuchi S., Tsuchiyama A., Nakano T. & Uesugi K. 2009: Magma deformation may induce non-explosive volcanism via degassing through bubble networks. *Earth and Planetary Science Letters* 281, 267–274. https://doi.org/10.1016/j.epsl.2009.02.036

Pálková H., Kureková V., Madejová J., Netriová Z., Uhlík P., Varga P., Hronský V. & Lexa J. 2020: Determination of water content in raw perlites: Combination of NIR spectroscopy and thermoanalytical methods. *Spectrochimica Acta Part A: Molecular and Biomolecular Spectroscopy* 240, 118517.

Peccerillo A. & Taylor S.R. 1976: Geochemistry of Eocene clac-alkaline volcanic rocks from the Kastamonu area, northern Turkey. *Contributions to Mineralogy and Petrology* 58, 63–81.

Pichler H. 1965: Acid hyaloclastites. *Bulletin Volcanology* 28, 293–310.

Putirka K.D. 2008: Thermometers and barometers for volcanic systems. In Putirka K.D & Tepley III F.J. (Eds.): Minerals, inclusions and volcanic processes. *Reviews in Mineralogy and Geochemistry* 69, 61–120.

Richey J.E. 1961: The Tertiary Volcanic District of Scotland. *British Geological Survey*, Edinburgh, 1–103.

Ross C.S. & Smith R.L. 1955: Water and other volatiles in volcanic glass. *American Mineralogist* 40, 1071–1089.

Rottier B., Audétat A., Koděra P. & Lexa J. 2020: Magmatic evolution of the mineralized Štiavnica volcano (Central Slovakia): Evidence from thermobarometry, melt inclusions, and sulfide inclusions. *Journal of Volcanology and Geothermal Research* 401, https://doi.org/10.1016/j.jvolgeores.2020.106976

Roulia M. Chassapis K., Kapoutsis J.A., Kamitsos E.I. & Savvidis T. 2006: Influence of thermal treatment on the water release and the glassy structure of perlite. *Journal of Materials Science* 41, 5870–5881.

Scutter C.R., Cas R.A.F., Moore C.L. & de Rita D. 1998: Facies architecture and origin of a submarine rhyolitic lava flow-dome complex, Ponza, Italy. *Journal of Geophysical Research: Solid Earth* 103, 27551–27566.

Seghedi I. & Downes H. 2011: Geochemistry and tectonic development of Cenozoic magmatism in the Carpathian–Pannonian region. *Gondwana Research* 20, 655–672. https://doi.org/10.1016/j.gr.2011.06.009

Selingman A.N., Bindeman I.N., Watkins J.M. & Ross A.M. 2016: Water in volcanic glass: From volcanic degassing to secondary hydration. *Geochimica et Cosmochimica Acta* 191, 16–238. https://doi.org/10.1016/j.gca.2016.07.010

Shields J.K., Mader H.M., Caricchi L., Tuffen H., Mueller S., Pistone M. & Baumgartner L. 2016: Unravelling textural heterogeneity in obsidian: Shear-induced outgassing in the Rocche Rosse flow. *Journal of Volcanology and Geothermal Research* 310, 137–158. https://doi.org/10.1016/j.jvolgeores.2015.12.003

Singh M.M. 2020: Perlite. In: Mineral commodity summaries 2020. *U.S. Geological Survey*, 120–121. https://doi.org/10.3133/mcs2020

Stevenson R.J., Dingwell D.B., Bagdassarov N.S. & Manley C.R. 2001: Measurement and implication of "effective" viscosity

for rhyolite flow emplacement. *Bulletin of Volcanology* 63, 227–237. https://doi.org/10.1007/s004450100137

Stolper E. 1982: The speciation of water in silicate melts. *Geochimica et Cosmochimica Acta* 46, 2609–2620.

Šalát J. & Ončáková P. 1964: Perlites, their occurrence, petrochemistry and application. *Vydavateľstvo Slovenskej akadémie vied*, Bratislava, 1–147 (in Slovak).

Tsikouras B., Passa K.P., Iliopuulos I. & Katagas C. 2016: Microstructural control on perlite expansibility and geochemical balance with a novel application of isocon analysis: An example from Milos Island perlite (Greece). *Minerals* 6, 80.

Uhlík P., Varga P., Pálková H. & Lexa J. 2015: Water in perlite – thermal analysis. In: Jurkovič Ľ., Slaninka I. & Ďurža O. (Eds.): Geochémia 2015. *Štátny geologický ústav D. Štúra*, Bratislava, 163–165 (in Slovak).

Van Otterloo J., Cas R.A.F. & Scutter C.R. 2015: The fracture behaviour of volcanic glass and relevance to quench fragmentation during formation of hyaloclastite and phreatomagmatism. *Earth-Science Reviews* 151, 79–116. https://doi.org/10.1016/j.earscirev.2015.10.003

Varga P. 2018: The forms of water in the perlite from Jastrabá and Lehôtka pod Brehmi deposits. *PhD Thesis, Comenius University in Bratislava, Faculty of Natural Sciences, Department of Economic Geology*, 1–164 (in Slovak).

Varga P., Uhlík P., Lexa J., Šurka J., Bizovská V., Hudec P. & Pálková H. 2019: The influence of porosity on the release of water from perlite glass by thermal treatment. *Monatshefte für Chemie* 150, 1025–1040. https://doi.org/10.1007/s00706-019-02410-w

Von Aulock F.W., Nichols A.R.L., Kennedy B.M. & Oze C. 2013: Timescales of texture development in a cooling lava dome. *Geochimica et Cosmochimica Acta* 114, 72–80. https://doi.org/10.1016/j.gca.2013.03.012

Wadge G., Ryan G. & Calder E.S. 2009: Clastic and core lava components of a silicic lava dome. *Geology* 37, 551–554. https://doi.org/10.1130/G25747A.1

White J.D.L. & Houghton B. 2000: Surtseyan and related phreatomagmatic eruptions. In: Sigurdsson H., Houghton B.F., McNutt S.R., Rymer H. & Stix J. (Eds.): Encyclopedia of Volcanoes. *Academic Press*, San Diego, 495–511.

Williams H. 1932: The history and character of volcanic domes. *University of California, Department of Geological Sciences Bulletin* 21, 51–146.

Wohletz K.H. & Heiken G. 1992: Volcanology and Geothermal Energy. *University of California Press,* Berkeley, 1–413.

Wohletz K.H. & Sheridan M.F. 1983: Hydrovolcanic explosions II: evolution of basaltic tuff rings and tuff cones. *American Journal of Science* 283, 385–413.

Yanev Y. 2003: Petrology of Golobradovo perlite deposit, Eastern Rhodopes. *Geochemistry, Mineralogy and Petrology* 40, 1–20.

Yanev Y. 2008: Geology of the Eastern Rhodopes perlite deposits (Bulgaria): a review. In: Rudnyánszky P. (Ed.): Proceedings of the 6th Int. Conference and Exhibition on Perlites. *Szilikátipari Tudományos Egyesület*, Budapest, 177–195.

Zähringer K., Martin J. & Petit J. 2001: Numerical simulation of bubble growth in expanding perlite. *Journal of Material Science* 36, 2691–2705.

Zelenka T. 2013: Geology of the perlite bodies at Pálháza. *European Geologist* 36, 19–21.

Zhang Y. & Behrens H. 2000: H_2O diffusion in rhyolitic melts and glasses. *Chemical Geology* 169, 243–262.

Zhang Y., Xu Z., Zhu M. & Wang H. 2007: Silicate melt properties and volcanic eruptions. *Reviews of Geophysics* 45, RG4004.

Zotov N., Yanev Y., Epelbaum M. & Konstantinov L. 1992: Effect of water on the structure of rhyolite glasses – X-ray diffraction and Raman spectroscopy studies. *Journal of Non-Crystalline Solids* 142, 234–246.

Zuberec J. & Sýkora J. 1976: Lehôtka pod Brehmi – Starý Háj perlite deposits: Preliminary and detail exploration – final report and reserves assessment. *Open file report, Archive of the State Geological Institute of D. Štúr*, Bratislava, 1–91 (in Slovak).

Zuberec J., Hroncová Z., Sýkora J. & Valko P. 1980: Lehôtka pod Brehmi and Jastrabá perlite deposits – Central Slovakia Volcanic Field: Final report and reserves assessment. *Open file report, Archive of the State Geological Institute of D. Štúr*, Bratislava, 1–127 (in Slovak).

Zuberec J., Tréger M., Lexa J. & Baláž P. 2005: Mineral resources of Slovakia. *Štátny geologický ústav D. Štúra*, Bratislava, 1–320 (in Slovak).

Electronic supplementary material is available online at:

Electronic supplement 1 "Methodology" at http://geologicacarpathica.com/data/files/supplements/GC-72-3-Lexa_Suppl1_methodology.docx

Electronic supplement 2 "Field documentation and lithology" at http://geologicacarpathica.com/data/files/supplements/GC-72-3-Lexa_Suppl2_field_documentation_lithology.docx

Electronic supplement 3 "Samples for laboratory investigation" at http://geologicacarpathica.com/data/files/supplements/GC-72-3-Lexa_Suppl3_samples.docx

Electronic supplement 4 "Mineral compositions" at http://geologicacarpathica.com/data/files/supplements/GC-72-3-Lexa_Suppl4_mineral_compositions.docx

Electronic supplement 5 "The results of X-Ray powder diffraction quantitative analyses from various types of perlite from Lehôtka pod Brehmi and Jastrabá deposits" at http://geologicacarpathica.com/data/files/supplements/GC-72-3-Lexa_Suppl5_XRD_analyses.xlsx

Electronic supplement 6 "Major and trace element composition of perlites from the Lehôtka pod Brehmi and Jastrabá deposits (monogenetic rhyolite volcanoes)" at http://geologicacarpathica.com/data/files/supplements/GC-72-3-Lexa_Suppl6_whole_rock_analyses.xlsx

Electronic supplement 7 "Microprobe analyses of hydrated glass in perlite samples from the Lehôtka pod Brehmi and Jastrabá deposits (monogenetic rhyolite volcanoes)" at http://geologicacarpathica.com/data/files/supplements/GC-72-3-Lexa_Suppl7_glass_EPMA_analyses.xlsx

Electronic supplement 8 "Plots of perlite and glass compositions" at http://geologicacarpathica.com/data/files/supplements/GC-72-3-Lexa_Suppl8_compositional_plots.docx

Electronic supplement 9 "Data on loss on ignition (LOI, 950 °C) and loss on drying (105 °C) of perlites and surrounding rocks from the Lehôtka pod Brehmi deposit" at http://geologicacarpathica.com/data/files/supplements/GC-72-3-Lexa_Suppl9_loss_on_ignition.xlsx